

PRELIMINARY STUDY OF THE MELTING LAYER IN THE TROPIC USING A POLARIMETRIC DOPPLER X-BAND RADAR

by

José J. Rosario Colón

A thesis submitted in partial fulfillment of the requirements for the degree of

MASTER OF SCIENCE
in
ELECTRICAL ENGINEERING

UNIVERSITY OF PUERTO RICO
MAYAGÜEZ CAMPUS
2013

Approved by:

Sandra L. Cruz-Pol, PhD
Member, Graduate Committee

Date

Leyda V. León Colón, PhD
Member, Graduate Committee

Date

José G. Colom Ustáriz, PhD
President, Graduate Committee

Date

Isabel Ríos López, MBA
Representative of Graduate Studies

Date

Pedro I. Rivera Vega, PhD
Chairperson of the Department

Date

ABSTRACT

In many parts of the world, the atmospheric melting layer affects the quantification of precipitation made by weather radars. The purpose of this study is to confirm the presence of the melting layer in the Caribbean Tropic using a ground-based radar. Some of the characteristics of the melting layer, such as the height and width, are computed through algorithms developed in this work. A statistical analysis of the percentage of times the melting layer is present in the atmosphere during this study is also completed. Finally, with the statistical analysis and the characteristics of the melting layer, it is determined the necessity to incorporate algorithms in the TropiNet radars to correct for attenuation or errors in the quantification of precipitation caused by the melting layer.

RESUMEN

En muchas partes del mundo, la capa de fusión atmosférica afecta la cuantificación de precipitación hecha por radares meteorológicos. El propósito de este estudio es confirmar la presencia de la capa de fusión en el trópico del caribe utilizando un radar ubicado en tierra. Algunas de las características de la capa de fusión, como la altura y el diámetro, son calculadas a través de algoritmos desarrollados en este trabajo. Un análisis estadístico del porcentaje de veces que la capa de fusión está presente en la atmósfera durante este estudio es, también, completado. Finalmente, con el análisis estadístico y las características de la capa de fusión, se determina la necesidad de incorporar algoritmos en los radares TropiNet para corregir por atenuación o errores en la cuantificación de precipitación causada por la capa de fusión.

To God and my family...
Without them I would not be here.

But they that wait upon the Lord shall renew their strength;
they shall mount up with wings as eagles;
they shall run, and not be weary;
and they shall walk, and not faint.

Isaiah 40:31 KJV

ACKNOWLEDGEMENTS

During the development of my graduate studies in the University of Puerto Rico several persons and institutions collaborated directly and indirectly with my research. Without their support it would be impossible for me to finish my work. That is why I wish to dedicate this section to recognize their support.

I want to start thanking God for giving me the opportunity to live and having blessed my studies. I also thank my father, mother, brother, sister, grandparents, aunts, uncles, and my extended family, for their prayers, support, and motivation.

I would like to express my sincere acknowledgement to my advisor, José G. Colom Ustáriz and the members of my committee, Sandra L. Cruz-Pol and Leyda V. León Colón, for the opportunity of doing research with them and for the guidance and supervision. I also want to thank the people from the Cloud Microwave Measurements of Atmospheric Events (CLiMMATE) Laboratory at the University of Puerto Rico at Mayagüez for all the work and all the moments that we spent together. Thanks to my friends Wilson Castellano, José Cordero, Benjamin De Jesús, Keyla Mora, and José Ortiz because without them it would have been impossible to overcome the challenges of graduate studies.

Special thanks to Colorado State University (CSU) and CSU-CHILL staff, especially to Miguel Gálvez and Francesc Junyent, for the training with the TropiNet radars.

Finally, I want to be grateful to the ECE department professional counselor, Madeline Rodríguez, and the graduate academic counselor, Sandra Montalvo for their help and scolding when I needed the most. Also, I want to thank the UPRM R&D staff, especially to Moisés Arroyo, Evelyn Guzmán, and Leonides Ruiz for their help in all the situations indirectly related with my research. The Grant from NSF MRI ECCS-0821331 provided the funding and the resources for the development of this research.

Table of Contents

ABSTRACT	II
RESUMEN.....	III
ACKNOWLEDGEMENTS.....	V
TABLE OF CONTENTS	I
TABLE LIST	III
FIGURE LIST.....	IV
CHAPTER I.....	2
1 INTRODUCTION.....	2
1.1 OVERVIEW	2
1.2 SUMMARY OF FOLLOWING CHAPTERS	4
1.3 DATA SOURCES.....	4
1.3.1 TropiNet X-Band Weather Radar.....	4
1.3.2 Sounding.....	8
1.3.3 Radar Rain Events.....	9
1.4 RESEARCH OBJECTIVES	10
CHAPTER II.....	11
2 THEORETICAL BACKGROUND AND RELATED WORK.....	11
2.1 RADAR THEORY REVIEW	11
2.1.1 The Radar System and its subsystems	11
2.1.2 Weather Radar Products	16
2.2 MELTING LAYER.....	19
2.3 MELTING LAYER DETECTION TECHNIQUES	21
2.3.1 Vertical Bidirectional Sector Scan Technique	21
2.3.2 Vertically Pointing Non-scanning Technique	22
CHAPTER III.....	23
3 MELTING LAYER DETECTION AND ANALYSIS METHOD.....	23
CHAPTER IV	28
4 RESULTS OF THE MELTING LAYER ANALYSIS.....	28
4.1 STRONG CONVECTIVE RAIN EVENT	30
4.2 LIGHT RAIN EVENT	34
4.3 MIXED MODERATE RAIN EVENT	39
CHAPTER V.....	44
5 CONCLUSIONS	44
5.1 SUMMARY	44
5.2 FUTURE WORK.....	45
REFERENCES	47

APPENDIX	50
APPENDIX A: DATA PROCESSING PROGRAM SOURCE CODE	50
APPENDIX B: VERTICAL PROFILE OF REFLECTIVITY PROGRAM SOURCE CODE	58

Table List

Tables	Page
Table 1.1 Radar Specifications	8
Table 4.1 Average Characteristics of the Melting Layer (m)	28
Table 4.2 Average Characteristics of the Melting Layer for July 31 st , 2012 Rain Event (m)	31
Table 4.3 Average Characteristics of the Melting Layer for August 24 th , 2012 Rain Event (m)	35
Table 4.4 Average Characteristics of the Melting Layer for August 25 th , 2012 Rain Event (m)	40

Figure List

Figures	Page
Figure 1.1 Data taken on June 8, 2011 with the radar CSU_X25P at Mayagüez, PR. (a) Reflectivity Range Height Indicator scan with the melting layer at 4.1 km of altitude. (b) Reflectivity Plan Position Indicator scan showing the shower where the melting layer was found.	3
Figure 1.2 Range and Location of TropiNet-1 Radar	5
Figure 1.3 3D drawing of the TropiNet Radar	7
Figure 2.1 Basic operation of the weather radar (Mora, 2012)	12
Figure 2.2 Simplified block diagram of a radar	13
Figure 2.3 Simple representation of the bright band (melting layer)	20
Figure 3.1 Flow chart of the computational process	25
Figure 3.2 General form of the Vertical Profile of Reflectivity	26
Figure 4.1 Reflectivity PPI and RHI respectively, taken on September 14 th , 2012 with TropiNet-1 radar	29
Figure 4.2 (a) Corrected reflectivity RHI scan with melting layer present, (b) close-up of the same RHI scan from the July 31 st , 2012 rain event	31
Figure 4.3 (a) Cross-polar correlation RHI scan with melting layer present, (b) close-up of the same RHI scan from the July 31 st , 2012 rain event	32
Figure 4.4 (a) Corrected differential reflectivity RHI scan with melting layer present, (b) close-up of the same RHI scan from the July 31 st , 2012 rain event	33
Figure 4.5 (a) Specific differential phase RHI scan with melting layer present, (b) close-up of the same RHI scan from the July 31 st , 2012 rain event	33
Figure 4.6 (a) Corrected reflectivity RHI scan with melting layer present, (b) close-up of the same RHI scan from the August 24 th , 2012 rain event	34
Figure 4.7 (a) Cross-polar correlation RHI scan with melting layer present, and (b) close-up of the same RHI scan from the August 24 th , 2012 rain event	36
Figure 4.8 (a) Corrected differential reflectivity RHI scan with melting layer present, and (b) close-up of the same RHI scan from the August 24 th , 2012 rain event	36
Figure 4.9 (a) Specific differential phase RHI scan with melting layer present, and (b) close-up of the same RHI scan from the August 24 th , 2012 rain event	37
Figure 4.10 (a) PPI scan of the corrected reflectivity, (b) PPI scan of cross-polar correlation, (c) PPI scan of corrected differential reflectivity, and (d) PPI scan of specific differential phase from the August 24 th , 2012 rain event	38
Figure 4.11 (a) Corrected reflectivity RHI scan with melting layer present, (b) close-up of the same RHI scan from the August 25 th , 2012 rain event	39
Figure 4.12 (a) Cross-polar correlation RHI scan with melting layer present, and (b) close-up of the same RHI scan from the August 25 th , 2012 rain event	41
Figure 4.13 (a) Corrected differential reflectivity RHI scan with melting layer present, and (b) close-up of the same RHI scan from the August 25 th , 2012 rain event	41

Figure 4.14 (a) Specific differential phase RHI scan with melting layer present, and (b) close-up of the same RHI scan from the August 25th, 2012 rain event 42

Figure 4.15 (a) PPI scan of the corrected reflectivity, (b) PPI scan of cross-polar correlation, (c) PPI scan of corrected differential reflectivity, and (d) PPI scan of specific differential phase from the August 25th, 2012 rain event 43

CHAPTER I

1 INTRODUCTION

1.1 Overview

For the Caribbean Tropic, there is no evidence in the literature of studies concerning the melting layer using ground-based radars. Often, scientist had opted to neglect the presence of the melting layer in the tropics, since it might be too high in the atmosphere to affect radar measurements. But recent observations with the UPRM X-Band radar indicate that the melting layer can be low enough that its effects on radar measurements should be considered. Figure 1.1¹ shows one of the first melting layer images measured with the ground based X-band radar in the western coast of Puerto Rico. Therefore, this study is of great importance for the region, since it will help to properly correct implementation of new weather radars working in the X-Band, and other frequency bands as well. The attenuation caused by the melting layer at X-Band is equivalent to 10 km of rain that is present below it and it can cause severe limitations to the sensitivity of the sensor system (*Bellon et al.*, 1997). This attenuation can be corrected with a vertical profile of reflectivity (VPR) approach as a correction method (*Matrosov et al.*, 2007).

¹ Image provided by Miguel Gálvez.

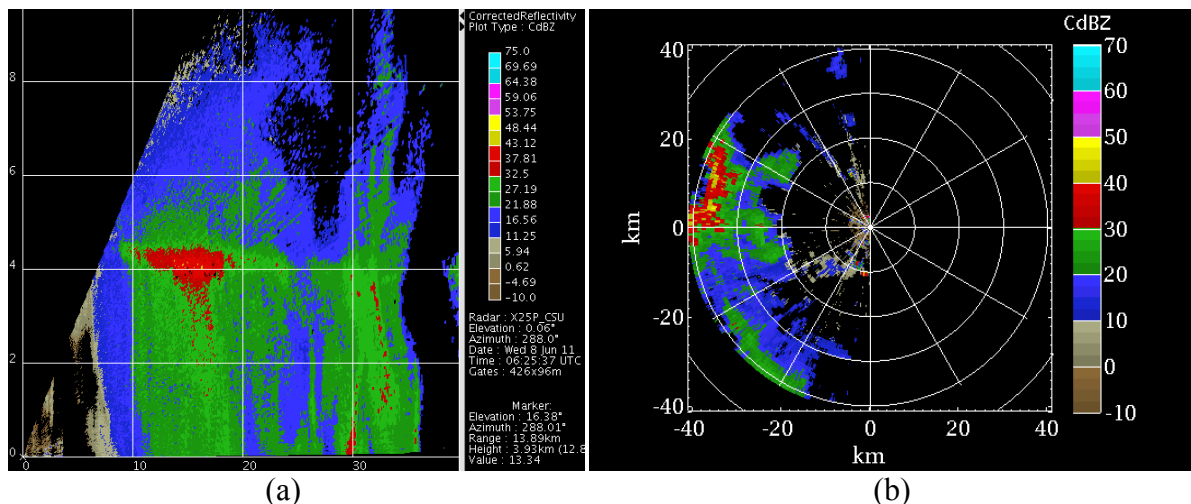


Figure 1.1 Data taken on June 8, 2011 with the radar CSU_X25P at Mayagüez, PR. (a) Reflectivity Range Height Indicator scan with the melting layer at 4.1 km of altitude. (b) Reflectivity Plan Position Indicator scan showing the shower where the melting layer was found.

In addition, the typical higher reflectivity measured by the radar, when looking at the melting layer, results in excessive estimation of the accumulated water on the ground, a problem that has been observed before in the Puerto Rico's west coast with the use of long-range radars (i.e. NEXRAD). The over estimation creates discrepancies between the readings of the radar and other sensors deployed on the ground, making it more difficult for the scientists to create new precipitation models and properly calibrate the system.

This work intended to verify that the melting layer is formed under specific conditions in the Caribbean Tropic at an altitude that can affect radar reflectivity measurements. Once it is proved that the melting layer is present, some of the characteristics of the melting layer are provided.

1.2 Summary of Following Chapters

Five chapters comprise this thesis. Chapter 1 introduces the subject of this thesis. This chapter also describes the various equipment and data sources used during the last couple of years to achieve our goal, and the objectives of the study. Specific history, theory, and techniques to detect the melting layer are discussed in Chapter 2. In Chapter 3, the detection method and the analysis performed to study the melting layer are discussed. The results of this analysis are presented in Chapter 4 including the study cases where the melting layer was found. Chapter 5 includes the conclusions derived from the results discussed in the previous chapter and suggestions for future research.

1.3 Data Sources

The characteristics of the first X-Band Doppler Dual-Polarized radar installed in Puerto Rico as well as the availability of auxiliary sensors used to complete this work are discussed.

1.3.1 TropiNet X-Band Weather Radar

The main instrument used to accomplish our objectives is the first TropiNet radar, deployed in the western coast of Puerto Rico. This radar, called TropiNet-1, is a state of art, low power, short range X-Band Doppler radar with dual linear polarization. TropiNet-1 was deployed in Cornelia Hill, located in Cabo Rojo, Puerto Rico, with coordinates lat. 18.16236N, long. 67.17773W. Figure 1.2 shows the location and coverage of the radar. The TropiNet-1 maximum range is 40 km and the tower on which the radar is mounted is fifty feet (50') high.

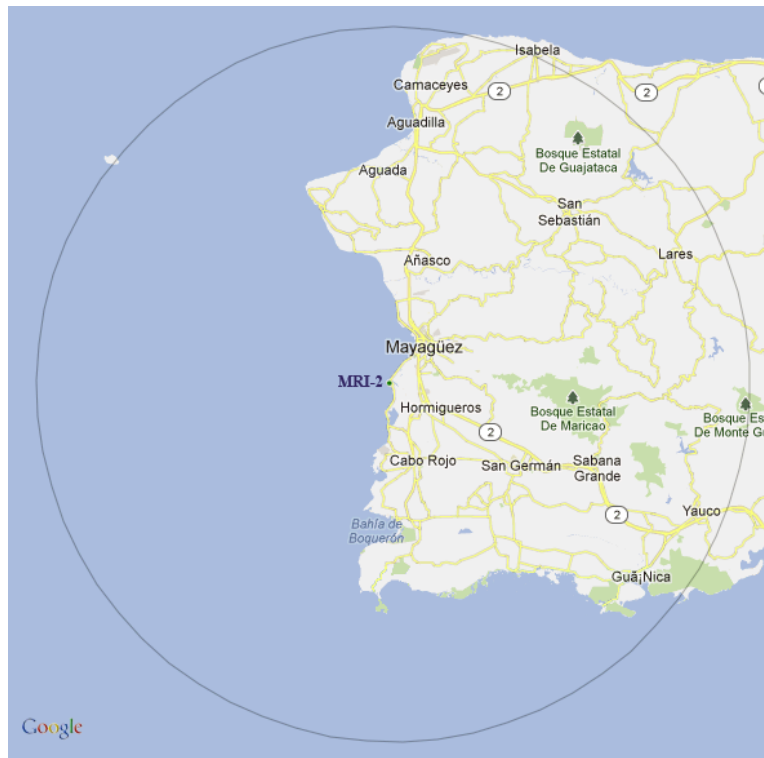


Figure 1.2 Range and Location of TropiNet-1 Radar

The radar is mounted on a cylindrical pole pedestal that has the elevation over its azimuth that will move the covered parabolic antenna. The transceiver is attached to the lateral frame arm to act as a counterweight for the antenna, shown in Figure 1.3. The pedestal control system, and the transceiver are accessed via Ethernet from the main computer of the radar (*Gálvez et al.*, 2009). The computer of the radar is connected to the Internet through a point-to-point wireless link from Cornelia Hill to the R&D Building in the University Campus, where the main server is located.

The transceiver uses a relatively low cost magnetron transmitter, fed to the antenna by a high isolation dual-channel duplexer. To ensure the maximum accuracy in estimating its

frequency, phase, power and duration of the transmitted signal, a sample of the pulse is fed to the receiver through a dedicated coupling path. The receiver has only one down-converting stage that is programmable and capable of tracking the magnetron's frequency across the entire bandwidth. To assure the overall coherency of the system the receiver is phase-locked to the data acquisition system. The data acquisition system has an Automatic Frequency Control (AFC) based on a Numerically Controlled Oscillator (NCO).

The antenna is a six feet (6') diameter dual-polarized center fed reflector, as shown in Figure 1.3. Only the dish is covered with a radome to reduce the water/ice build-up and wind loading on the reflector as opposed to a full radome covering the whole system, however no ice accumulation is expected in the tropics. The connectors of the dual-polarization scalar feeder are extended to the back of the reflector through two waveguide segments that supports the H and V polarizations.



Figure 1.3 3D drawing of the TropiNet Radar (*Galvez et al.*, 2009)

The pedestal has digital drive servomotors with digital absolute position encoders. To provide all the necessary signals (power, Ethernet, GPS) from the pedestal base to the transceiver, a slip ring assembly in the azimuth section is used. The one Gigabit (1Gb) Ethernet connection, the pedestal control link, and the main power connection are housed at base of the pedestal in an electrical cabinet.

A computer is dedicated to the Motion Control Unit (MCU) of the radar. This unit receives and interprets high-level motion commands and converts them to motor drive programming instructions. These instructions are then sent over the RS-232 link between the MCU and the servomotors on the pedestal. The MCU utilizes the same RS-232 link to obtain the antenna position, and then distribute the position data through its Ethernet interface to all connected clients. Other important specifications of the radar are in the Table 1.1. (*Gálvez et al.*, 2009)

Table 1.1 Radar Specifications

TRANSMITTER	
Type	Magnetron
Center Frequency	9410 +/- 30 MHz
Peak Power Output	8.0 kW (per channel)
Average Power Output	12 W (per channel)
Pulse Width	660-1000 ns
Polarization	Dual Linear, H and V
Max. Duty Cycle	0.16%
ANTENNA	
Type (Diameter)	Dual-polarized parabolic Reflector (1.6m)
3-dB Beam Width	1.4 deg
Gain	41 dB
Max. Scan Rate	60 deg/s
RECEIVER	
Type	Parallel, dual channel, linear output I/Q
Dynamic Range	95 dB (BW = 1.0 MHz)
Noise Figure	5 dB
DATA ACQUISITION SYSTEM	
Sampling Rate	200 Msps
Dynamic Range	105 dB (BW = 1.0 MHz)
Data Transfer Rate	88.3 MBps
Decimation Factor	Adjustable
Video Bandwidth	Adjustable

1.3.2 Sounding

In order to validate the height of the 0°C isotherm, sounding data from the area was used. These radiosondes measure pressure, height, temperature, dew point, and relative humidity, among other parameters of the atmosphere. The sounding data was acquired from (*Oolman,*

2012). By obtaining the 0°C isotherm altitude with the radiosonde, radar melting layer elevation measurements can be compared and provide assurance that the radar is properly working.

1.3.3 Radar Rain Events

Several rain events between June and October 2012 were analyzed for the purpose of this study. From the many observations, only three particular events show characteristics that deserve special attention and therefore, they are discussed in detail below.

1.3.3.1 Strong Convective Rain Event

The dataset obtained from TropiNet-1 X-band radar on July 31st, 2012 around 23:52:53 UTC, correspond to a dying thunderstorm that reached reflectivity values in the order of 50dBZ.

1.3.3.2 Light Rain Event

The dataset obtained from TropiNet-1 X-band radar on August 24th, 2012 around 19:31:18 UTC, correspond to a light rain event that reached reflectivity values in the order of 30dBZ.

1.3.3.3 Mixed Moderate Rain Event

The dataset obtained from TropiNet-1 X-band radar on August 25th, 2012 around 04:08:17 UTC, correspond to a mixed rain event that reached reflectivity values in the order of 50dBZ.

1.4 Research Objectives

The main goal of this project is to determine the presence of the melting layer in the Caribbean Tropic. Once detected, we will provide the information to achieve the secondary objectives of the project, which is to determine:

- The average height of the melting layer's top and bottom
- The average thickness of the melting layer
- The melting layer formation occurrence rate for the period of the study
- The necessity to apply attenuation correction algorithms

The results will be mainly used in the improvement of the future TropiNet Radar Network being deployed in the western coast of Puerto Rico, and could serve as well to the National Weather Service (NWS) Office in San Juan, Puerto Rico.

CHAPTER II

2 THEORETICAL BACKGROUND AND RELATED WORK

2.1 Radar Theory Review

2.1.1 *The Radar System and its subsystems*

Radar is a system used to detect and locate reflecting targets. In this work, a weather radar with polarimetric, Doppler, monostatic, and pulsed characteristic is implemented to measure the reflectivity from hydrometeors. The radar detects its target by sending an electromagnetic signal, which is modulated, and then waits a period of time for the reflected signal to get back to the radar. In a monostatic pulsed radar the reflected signal enters through the same antenna that was used for transmission. Once the reflected signal is acquired it is compared with the transmitted signal to determine its location and other information related to the target (*Skolnik, 2001*).

To better understand the principles of operation of the radar refer to Figure 2.1. The transmitter sends a pulse to the atmosphere through the antenna. Once the transmitted pulse hits the target it is scattered in many directions. In this case the target is a sample volume of the atmosphere may contain hydrometeor particles such as rain, hail, snow, among others or a mixture of these. Part of the scattered pulse returns to the radar. The received signal is then processed and finally displayed to the end user. Figure 2.1 also presents an example of how the processed data is showed in a radar display; however, before the data collected by the radar is

presented to the user it needs to be processed. This brings our attention to the components of the radar.

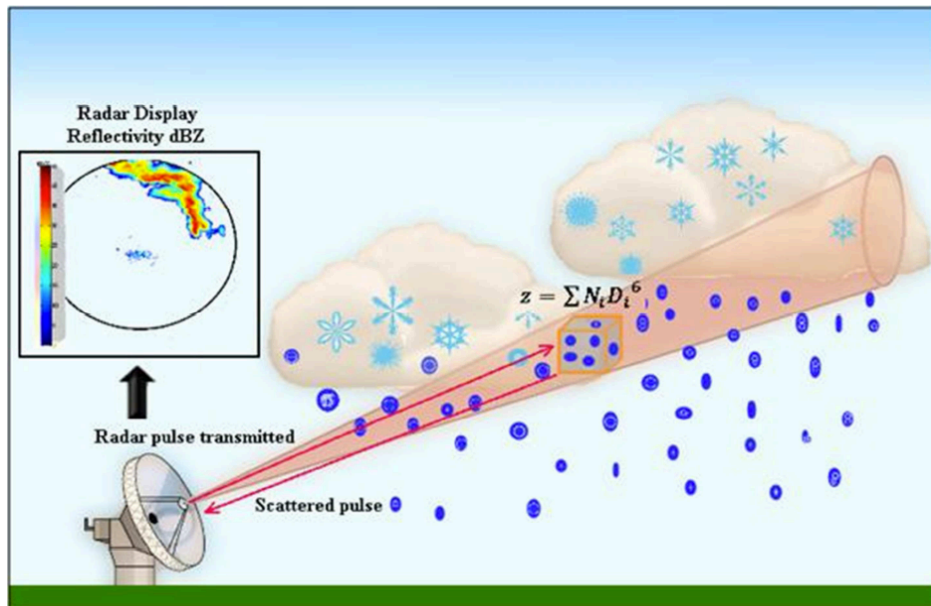


Figure 2.1 Basic operation of the weather radar (Mora, 2012)

The radar is composed of many subsystems integrated together. The basic subsystems in weather radars are the transmitter, antenna, receiver, signal processor, and display. Figure 2.2 shows the simplified block diagram of a radar.

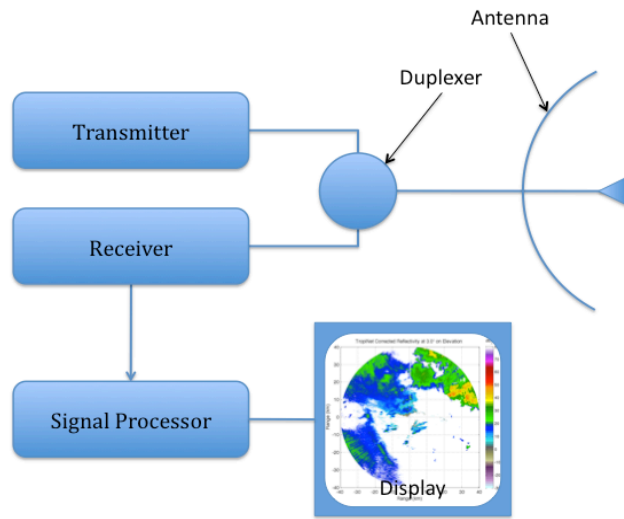


Figure 2.2 Simplified block diagram of a radar

The transmitter is the source of electromagnetic radiation of the radar. The range of frequencies of the electromagnetic signal sent by typical weather radars is from three to thirty five Gigahertz (3 to 35 GHz). The components that make up the transmitter are basically the waveform generator, modulator, and power amplifier. The waveform generator generates the low power signal to be transmitted (*Skolnik, 2001*). Normally it is an oscillator. The basic function of the modulator is to tell the transmitter when to transmit and for how long. In some radars it also stores energy between pulses so it will have more energy available for the next transmitted pulse. The three most common types of radar transmitters are the magnetron, klystron amplifier, and solid-state amplifier. The magnetron is a microwave generator, developed by Henry Boot and John Randall in 1939 (*Buderi, 1996*), composed of a series of resonant cavities, a cathode, and an anode. The power of the signal produced by a magnetron can exceed one megawatt (1MW). The klystron amplifier has a disadvantage over the other two amplifiers and is its large size. The klystron is considerably larger than the magnetron and the solid-state amplifier. On the other

hand, with the klystron is easier to control the transmitted pulse waveform and can also transmit more power, making it more attractive for coherent radar implementation. The downside of the solid-state amplifier is the low power they emit, although they are very suitable for radars with phased-array antennas. (*Rinehart, 2010*)

The purpose of the antenna is to send the transmitted signal from the transmitter to the atmosphere and send the received signal to the receiver. The antenna is connected to the transmitter and receiver through waveguides and a duplexer (transmit/receive switch). Waveguides are used instead of coaxial cables due to their low losses at microwave frequencies. Radars normally use directional antennas. There are many types of directional antennas. The most common are phased array, slotted waveguide, and parabolic antenna. A main circular parabolic reflector and a feed horn or a dipole with a sub-reflector forms the last one, usually used in weather radars.

The receiver is basically comprised of a low noise RF (radio frequency) amplifier, a mixer, an IF (intermediate frequency) amplifier, a matched filter, and a demodulator. The first component of the receiver is usually the RF amplifier. An amplifier is needed due to the weak signals received by the antenna. It has to be a low-noise amplifier because introducing more noise to the signal will make the data impossible to retrieve. After it is amplified, the received signal is mixed with a signal generated by a local oscillator (LO) to lower its frequency to make it more manageable. This frequency is called IF. If necessary, an IF amplifier is added so the data does not get lost. The mixing process of the received signal introduces unwanted noise to the

signal. To remove the unwanted noise it is necessary to clean the received signal with a matched filter. The adjective matched means that the filter frequency response is designed replicating the characteristics of the transmitted signal to maximize the signal-to-noise ratio (SNR) of the received signal. The demodulator, a crystal diode, extracts the information from the received signal and sends it to the signal processor (*Skolnik, 2001*).

Modern radars use computers as signal processors allowing the user to further process the data. Processing the data through algorithms that run a series of instructions to see if an event contains specific characteristics, for example the potential of a tornado to spawn. If the algorithm finds these characteristics, it indicates that a definite event is occurring and can emit a warning, which disseminated through the appropriate channels can save lives and property (*Rinehart, 2010*).

The display is a component of the radar that allows the user to have a visual image and interpretation for what the radar is detecting. The most simple radar display is called A-scope. It is basically an oscilloscope where the vertical axis represents the intensity of the signal and the horizontal axis represents time. Since we know the electromagnetic waves travel at approximately the speed of light in clear air, the horizontal axis scale can be transformed from time into distance. Unfortunately this type of display does not tell us where the target is, so to provide the position of the target the Plan Position Indicator (PPI) display was invented. The data presented in a PPI display is like presenting the data on top of a map, with the radar usually at the center of it. In the PPI display, rings determine the distance from the radar as polar

coordinates are used to determine position and the strength of the signal is represented by different colors. Another useful display for weather radars is the Range Height Indicator (RHI) display. As in the A-scope, the horizontal axis in the RHI display is distance from the radar. The vertical axis is height above the radar and the strength of the signal is represented in the same way as the PPI display. An example of a RHI and a PPI display can be seen in Figure 1.1 (a) and (b) respectively.

2.1.2 Weather Radar Products

The *reflectivity factor* (z) is one of the most common quantities measured by weather radars (Rinehart, 2010). This measurement is calculated from the raw data of the radar. In Equation 2.1 and Figure 2.1, above the sample volume cube, the reflectivity factor equation can be found; where N_i is the number of drops in the radar beam volume and D_i is the drop diameter.

$$z = \sum N_i D_i^6 \quad 2.1$$

The unit of z in linear scale is mm^6/m^3 , but it is normally presented in the logarithmic scale where dBZ is the unit. To change the values of z to its logarithmic scale, the Equation 2.2 is used.

$$dBZ = 10 \log_{10}(z) \quad 2.2$$

The problem with the Equation 2.1 is that the density of water droplets needs to be known in order to compute the reflectivity factor. To avoid this situation, is better to use an equation based on characteristics of the radar. This formula is expressed in Equation 2.3 where C is a constant, P_r is the received power (in Watts), and r is the distance from the radar (in meters).

$$z = CP_r r^2 \quad 2.3$$

This formula is based on the radar characteristics contained in the constant C . This constant is called the “radar constant” and is given by Equation 2.4. The characteristics of the radar on this formula are: λ is the wavelength of the signal transmitted by the radar, τ is the time “width” of the radar pulse, P_t is the peak power transmitted by the radar (in Watts), G is the radar antenna gain, θ is the azimuth beamwidth, and ϕ is the elevation beamwidth. The units of θ and ϕ are radians. Other elements of the equation are: $\ln(2)$ that is a correction for the antenna Gaussian beam approximation, K is the complex dielectric factor of the target, and c is the speed of light (3×10^8 m/s).

$$C = \frac{1024 \ln(2) \lambda^2}{\pi^3 |K|^2 c \tau P_t G^2 \theta \phi} \quad 2.4$$

Dual-polarized radars, which are radars capable of transmitting and receiving two polarizations, e.g. vertical and horizontal, are gaining popularity in weather applications. The *differential reflectivity* (Z_{DR}) is probably the most commonly used product of dual polarization

(Seliga & Bringi, 1976). There are two techniques to calculate Z_{DR} . These are the alternate or switched technique and the simultaneous technique. The alternate technique uses one transmitter and one receiver. It transmits one polarization at a time switching the polarization between pulses. The simultaneous technique uses one or two transmitters and two receivers. The Equation 2.5 defines the differential reflectivity as

$$Z_{DR} = 10 \log_{10} \left(\frac{z_H}{z_V} \right) \quad 2.5$$

where z_H and z_V are the horizontal and vertical reflectivity respectively in linear scale (Rinehart, 2010). The unit of Z_{DR} is decibels (dB). If the horizontal reflectivity and the vertical reflectivity are in dBZ (logarithmic scale), the differential reflectivity can be calculated as in Equation 2.6 where Z_H and Z_V are the horizontal and vertical reflectivity respectively.

$$Z_{DR} = Z_H - Z_V \quad 2.6$$

The *differential phase* (Φ_{DP}) is the phase difference between the horizontal and vertical polarization signals. This difference is caused by the delay of the signal as it passes through the raindrops. If the raindrops were perfect spheres, Φ_{DP} would be zero. The *differential phase* is measured in degrees and is defined in Equation 2.7 as follows:

$$\phi_{DP} = \phi_{HH} - \phi_{VV} \quad 2.7$$

where Φ_{HH} is the phase of the signal transmitted and received by the horizontal polarization, and Φ_{VV} is the phase of the signal transmitted and received by the vertical polarization. The differential phase is not very useful because of its dependence on distance from the radar (Rinehart, 2010). The *specific differential phase*, as explained below, is a more practical product.

The *specific differential phase* (K_{DP}) is basically the discrete derivative of Φ_{DP} . Orientation, index of refraction, shape, and hydrometeor size are the parameters on which the specific differential phase depends and it is not dependent on the beam blockage, transmitted power measurements errors or errors in the receiver calibration (Rinehart, 2010). K_{DP} is defined in Equation 2.8 and its unit is degrees/km.

$$K_{DP} = \frac{\phi_{DP}(r_2) - \phi_{DP}(r_1)}{2(r_2 - r_1)} \quad 2.8$$

2.2 Melting Layer

Ice crystals, snow or hail is the form that takes the moisture found in altitudes where the temperature is below freezing (Skolnik, 2001). These frozen particles undergo the transition from solid to liquid as they descend and the temperature rises above freezing. Melting from the outside in creates a layer of liquid water around the ice. When this occurs, the reflectivity in the radar readings increases. Reaching a maximum when the ice particle is completely covered with water, but it has not lost its initial form. Then the reflectivity readings start to decrease until the

transition from solid to liquid has completed. This process creates a band or strip of high reflectivity called “bright band”. A simple representation of the bright band is shown below in Figure 2.3.

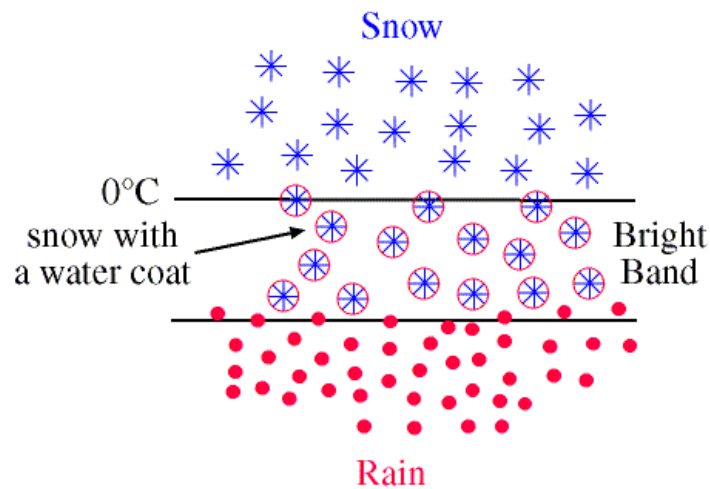


Figure 2.3 Simple representation of the bright band (melting layer) (*Atkins, 2002*)

In physics and meteorology the bright band is called the “melting layer”. When present, its height can vary from a few hundred meters to several kilometers depending on the region and season. The melting layer is found at an altitude where the temperature is just above 0°C. From one to four hundred meters (100 to 400 m) below the 0°C isotherm is where the center of the melting layer is found (*Skolnik, 2001*). The reflectivity in the center of the melting layer, what is called the bright band height, is generally six to ten decibels (6 to 10 dB) greater than the reflectivity of the rain below it and twelve to fifteen decibels (12 to 15 dB) greater than the ice particles above it (*Battan, 1973*). Rainfall estimation with radar data can be overestimated, sometimes by as much as a factor of five (5), if the melting layer is present but not acknowledge (*Tan & Goddard, 1995*).

Since the end of the World War II radars have turned out to be a very valuable tool to observe the weather (*Battan, 1962*). The melting layer has been observed since the beginning of radar meteorology (*Cunningham, 1947; Marshall et al., 1947*). This is due to its relevance for retrieval of the 0°C isotherm (*White et al., 2002*), quantitative radar rainfall estimation (*Smyth & Illingworth, 1998*), and hydrometeor classification (*Hongping & Chandrasekar, 2000*). The polarimetric radar signatures of the bright band have been widely studied; after Browne and Robinson began to make cross-polarization observations of the melting layer in 1952 (*Bringi & Chandrasekar, 2001*). But, the first measurements of the bright band made with a Doppler radar were published in (*Lhermitte & Atlas, 1963*).

2.3 Melting Layer Detection Techniques

For the purpose of this study, two different techniques to detect the melting layer were considered; vertical bidirectional sector scan technique and vertically pointing non-scanning technique. These detection techniques are described next.

2.3.1 Vertical Bidirectional Sector Scan Technique

The Vertical Bidirectional Sector Scan technique consists of scanning the atmosphere horizontally at first, in a PPI scan mode. From the PPI scan the operator or the algorithm, depending if the operation of the radar is automated or not, decides where to perform vertical scans depending on the reflectivity intensity of the clouds or any other characteristic observed by the operator. In other words, from the PPI scan it is decided when and where an RHI scan it is

going to be performed. Then the data is saved for further processing. The procedure to process the data collected using this technique is discussed in chapter 3.

This technique is slightly more complicated to be implemented in the radar operation, especially if the process is automated; the algorithm to control the radar is complex. On the other hand, the procedure to process the data is simpler and the data consumes less space in the hard drive than in the next technique.

2.3.2 Vertically Pointing Non-scanning Technique

The Vertically Pointing non-scanning technique is more straightforward in terms of implementation for the radar operation. It consist on pointing the antenna of the radar straight to the sky toward zenith, i.e. ninety degrees (90°) on elevation, and start to save time series data for the duration of the study or rain event. Then process the data to extract the necessary information for the study or experiment.

The problem with this technique is the processing procedure is much more complicated and the time series data takes significantly more space in the hard drive. For example, time series data can occupy more than one Gigabyte (1 GB) of memory per minute compared with the data of the other technique that usually take less than one hundred Megabytes (< 100 MB) of memory per minute.

CHAPTER III

3 Melting Layer Detection and Analysis Method

Using the TropiNet-1, the atmosphere was vertically scanned. This allowed us to have a vertical cross section, to be displayed in a RHI. The RHI is a type of display that uses polar coordinates (range, elevation angle) to present the weather echoes. The horizontal axis of the RHI is the range or horizontal distance from the radar, while the vertical axis is height or altitude, which is the vertical distance from the radar. It is important to clarify that these distances are Above Ground Level (AGL). The value of the radar product is displayed in the RHI with a scale of colors. The color scale varies per product to easily identify each measurement by just looking at the plot.

The main products that will be used to identify the melting layer are going to be *corrected reflectivity* ($Z_H^{corrected}$), *cross-polar correlation* (ρ_{HV}), and *specific differential phase* (K_{DP}). Other radar products can be used to identify characteristics of the melting layer and some conditions that are needed for the melting layer to be formed, such as *velocity* (V), *differential reflectivity* ($Z_{DR}^{corrected}$), and *differential phase* (ϕ_{DP}).

First the data was analyzed in a real-time display to identify the melting layer. This analysis preliminary consisted of the operator watching the radar display in real-time to detect the presence of the bright band in the scan. In the event that the operator is not present while the

radar is in operation all the data is saved through an automated script. Once the data was saved, it was post-processed running a MatLab script. This program, which source code is available in Appendix A, uses first a simple technique to correct the data for attenuation. The attenuation correction technique used in this program is found in Chapter 7 of (*Bringi & Chandrasekar, 2001*). After the data is corrected for attenuation, it is filtered. Two filters are used, the first one filters the first three gates and the second one filters the uncorrelated data. After the data is corrected and filtered, the elevations are compared to decide if the scan is a PPI or a RHI scan. The adequate plane to plot the data is selected and created. Then the *corrected reflectivity*, *corrected differential reflectivity*, *cross-polar correlation*, and *specific phase* are plotted and saved. When all the data is processed, the presence of the melting layer is confirmed with the data obtained from the radiosonde and the *cross-polar correlation* from the radar itself.

Those scans where the melting layer is present were separated for further processing with computational software to identify the characteristics of the melting layer. First the computational software, a MatLab script which source code is in Appendix B, uses the same attenuation correction technique as the other script to correct the data for attenuation. Then verifies that the file to process is a RHI scan because, for this procedure, the only files that should be processed are RHI scans. After verifying the file, the adequate plane to plot the data is selected and created. Next the Vertical Profile of Reflectivity (VPR) is generated and filtered. Then the VPR is plotted and saved. The characteristics of the melting layer such as top height, melting layer height, bottom height, and melting layer width were extracted with the data cursor tool in MatLab. Figure 3.1 shows a flow chart of the previously discussed process.

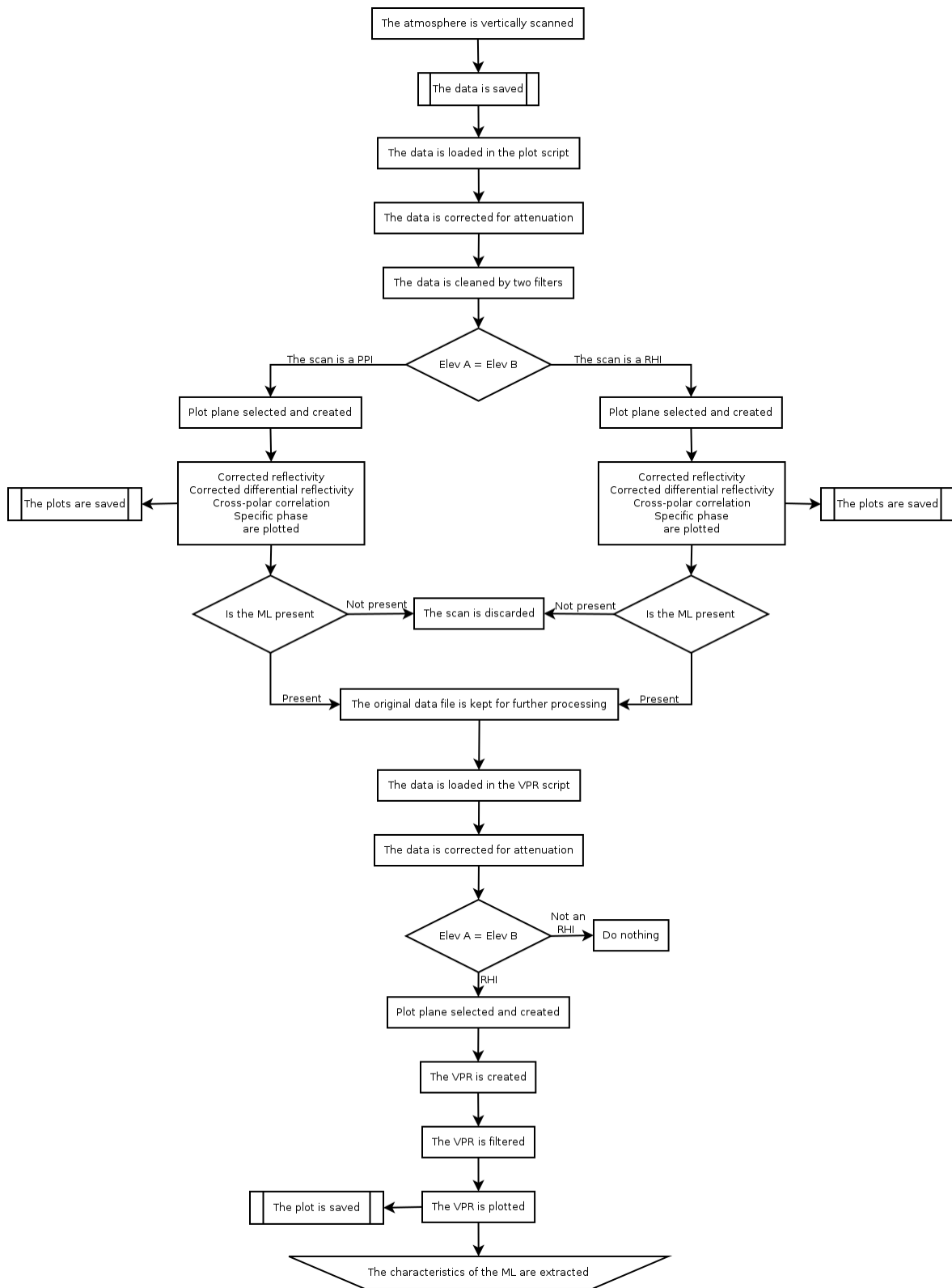


Figure 3.1 Flow chart of the computational process

Once the data recollection period was ended, all the data was processed and all the characteristics of the melting layer extracted, a statistical study of how often the melting layer forms in the Caribbean Tropic (western coast of Puerto Rico) was performed. The data recollection period was from June through October 2012. After the study, it was determined whether it was necessary to apply extra algorithms for attenuation correction and Quantitative Precipitation Estimation (QPE) correction for the data to be post-processed.

To apply the correction algorithm, first a set of RHI scans has to be recorded. The average of the RHI scans is computed to construct a VPR. Figure 3.2 shows the general signature of a VPR and defines some of the variables needed to apply the correction equations.

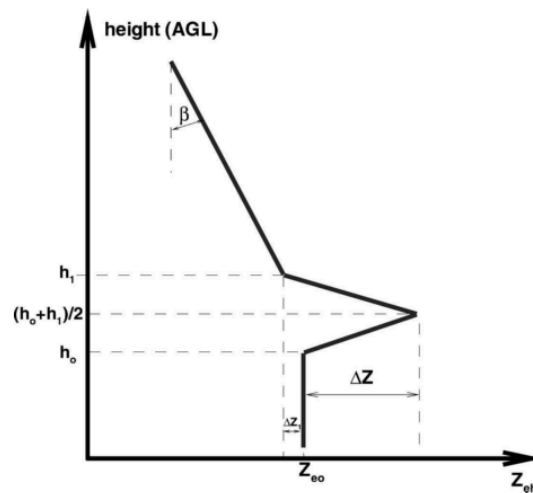


Figure 3.2 General form of the Vertical Profile of Reflectivity (*Matrosov et al., 2007*)

After the VPR is created, the reflectivity is defined by Equation 3.1 where $h = r \cdot \sin(\alpha)$ and the terms ΔZ , ΔZ_1 and $\tan(\beta)$ are defined from Figure 3.2 (Matrosov et al., 2007). Also note that $Z_H^{(a)}$ values are actually observed reflectivity and are already corrected for rain attenuation.

$$Z_H(r) = \begin{cases} Z_H^{(a)}(r) & \text{for } r \leq r_0, \\ Z_H^{(a)}(r) - 2\Delta Z(h - h_0)(h_1 - h_0)^{-1} & \text{for } r_0 < r \leq 0.5(r_0 + r_1), \\ Z_H^{(a)}(r) - \Delta Z + 2(\Delta Z + \Delta Z_1)(h - 0.5h_0 - 0.5h_1)(h_1 - h_0)^{-1} & \text{for } 0.5(r_0 + r_1) < r \leq r_1, \\ Z_H^{(a)}(r) + \Delta Z_1 + \tan(\beta)(h - h_1) & \text{for } r > r_1, \end{cases} \quad 3.1$$

CHAPTER IV

4 Results of the Melting Layer Analysis

The melting layer was observed three times during the period of this study. After analyzing all the data the characteristics of the melting layer discussed in the previous chapter were averaged. The average top height of the melting layer was four thousand seven hundred and thirteen meters (4,713 m). Four thousand six hundred and fourteen meters (4,614 m) was found to be the average melting layer height. The bottom height of the melting layer, in average, was four thousand five hundred and five meters (4,505 m). Subtracting the top height of the melting layer from its bottom height it is found that the average melting layer width is two hundred and eight meters (208 m). Table 4.1 summarizes these characteristics and includes the average height of the 0°C Isotherm, which was also used to corroborate the presence of the melting layer, and Figure 4.1 shows a PPI and a RHI scan of one of the rain events studied in which the melting layer was not found on a rain event that passed on September 14th, 2012.

Table 4.1 Average Characteristics of the Melting Layer (m)

ML Top Height	ML Height	ML Bottom Height	ML Width	0°C Isotherm Height
4,713	4,614	4,505	208	4,796

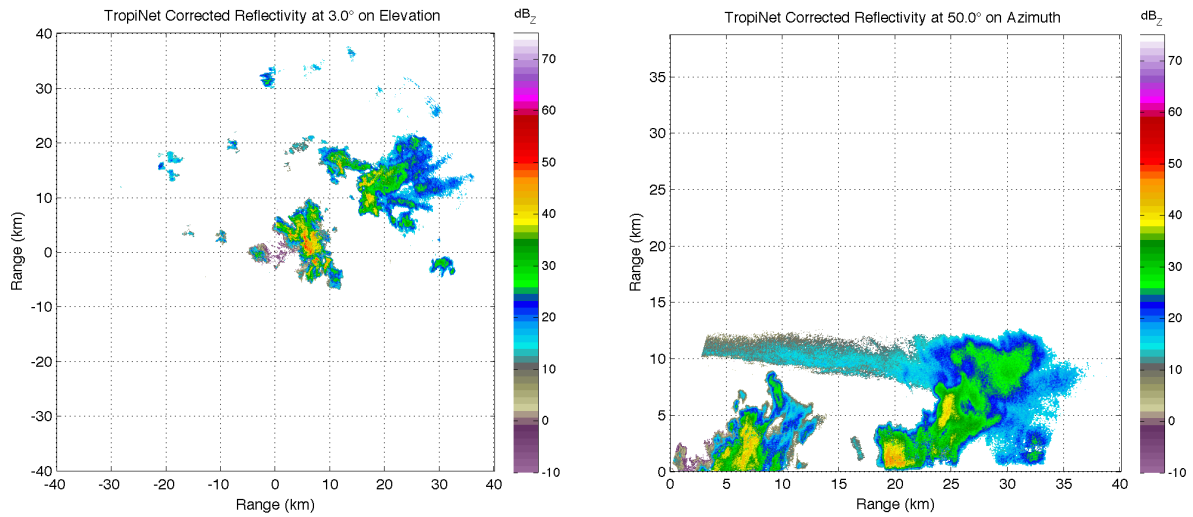


Figure 4.1 Reflectivity PPI and RHI respectively, taken on September 14th, 2012 with TropiNet-1 radar

Fifty (50) rain events were analyzed in this study, but only in three (3) occasions the melting layer was present. In contrast with the tropical region of India where the melting layer was present in twelve (12) of the fifty four (54) rain events recorded by TRMM in 2007 and eleven (11) of the thirty six (36) rain events recorded in 2008 (*Jaiswal et al.*, 2010). Jaiswal stipulates the melting layer was probably present in other occasions but the data was not recorded. Comparing the data of Jaiswal with the data obtained in this study, it can be seen that the occurrence of the melting layer in the Caribbean tropics was at least four times less than the melting layer occurrence in the tropical region of India.

In a study from 1998 to 2003 by (*Okamoto et al.*, 2004) also at a latitude of 18°, the average height of the melting layer was found to be 4,100 m. As presented before, in this study the average melting layer height is four thousand six hundred and fourteen meters (4,614 m), this

being five hundred meters (500 m) more than the average for our region around the globe. The next sections present the results of the three rain events where the melting layer was found.

4.1 Strong Convective Rain Event

This rain event occurred on July 31st, 2012 as described in Section 1.3.3.1. The melting layer was noticed around 23:52:53 UTC. Figure 4.2 (a) shows a reflectivity RHI scan of the rain event taken at 248.9° in azimuth. Figure 4.2 (b) shows a close-up of the same scan where the melting layer, identified with an ellipse, can be better appreciated. In this particular scan, the melting layer height is four thousand six hundred and eighty three meters (4,683 m).

The average top height of the melting layer for this event was four thousand eight hundred and sixty eight meters (4,868 m). The melting layer height on average for this event was found at four thousand seven hundred and sixty eight meters (4,768 m). The average melting layer bottom height was four thousand six hundred and fifty eight meters (4,658 m). The average melting layer width was calculated to be two hundred and ten meters (210 m).

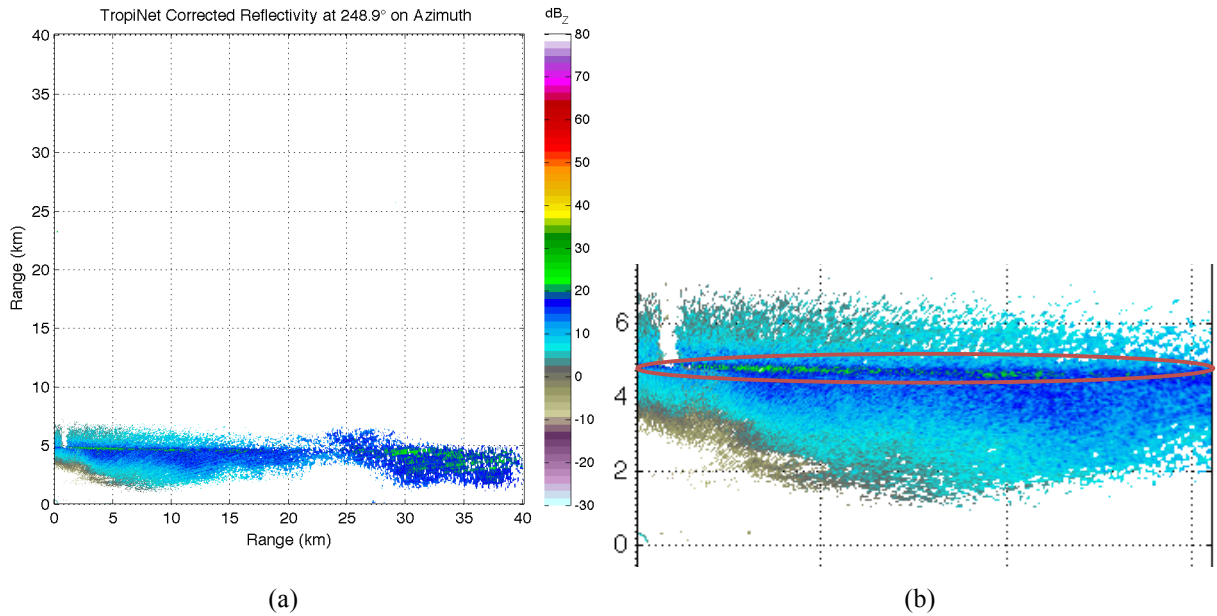


Figure 4.2 (a) Corrected reflectivity RHI scan with melting layer present, (b) close-up of the same RHI scan from the July 31st, 2012 rain event

The summary of the results is showed in Table 4.2 along with the 0°C isotherm height for this event.

Table 4.2 Average Characteristics of the Melting Layer for July 31st, 2012 Rain Event (m)

ML Top Height	ML Height	ML Bottom Height	ML Width	0°C Isotherm Height
4,868	4,768	4,658	210	4,886

The melting layer was corroborated using the cross-polar correlation, differential reflectivity, and specific differential phase of the data. Figure 4.3 (a) shows the cross-polar correlation of the same RHI scan presented in Figure 4.2. A close-up of the cross-polar correlation is showed in Figure 4.3 (b), where the drop in correlation of the data right in the

melting layer, identified with an ellipse, is better appreciated. In Figure 4.4 (a) it can be seen the corrected differential reflectivity. To appreciate better the positive change in differential reflectivity, Figure 4.4 (b) shows a close-up. The change in differential reflectivity was found to be between one and four decibels (1-4 dB). Figure 4.5 (a) shows the specific differential phase. The values found in the melting layer for the specific differential phase were between one and three degrees pre kilometer (1-3 °/km). In the close-up of the specific differential phase, shown in Figure 4.5 (b), the melting layer is marked with an ellipse.

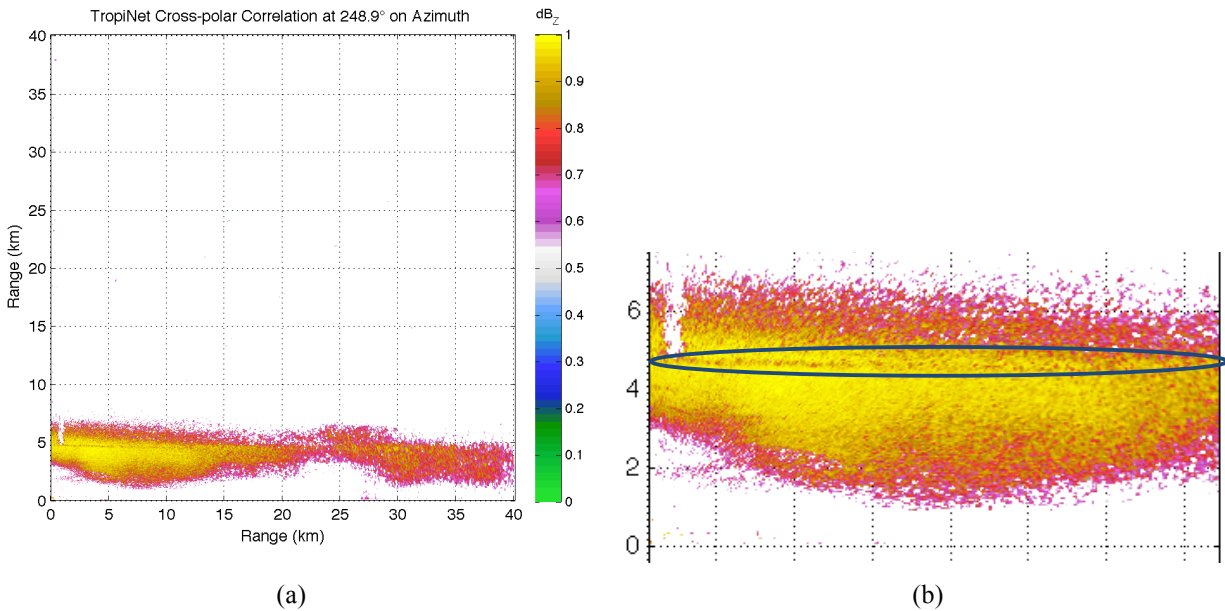


Figure 4.3 (a) Cross-polar correlation RHI scan with melting layer present, (b) close-up of the same RHI scan from the July 31st, 2012 rain event

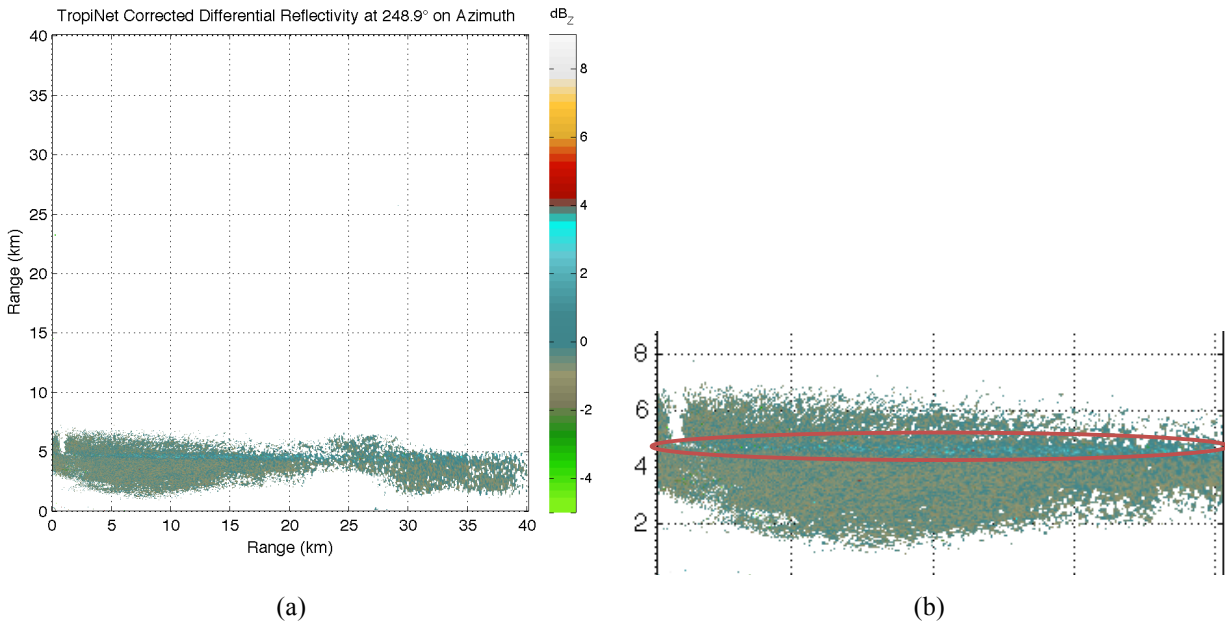


Figure 4.4 (a) Corrected differential reflectivity RHI scan with melting layer present, (b) close-up of the same RHI scan from the July 31st, 2012 rain event

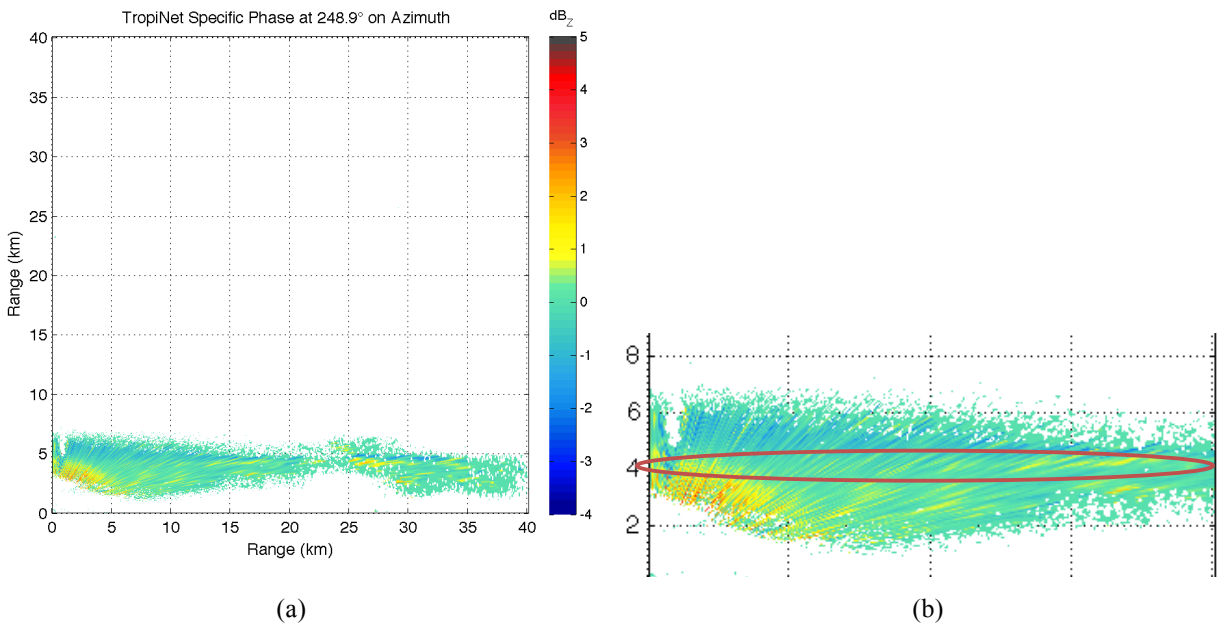


Figure 4.5 (a) Specific differential phase RHI scan with melting layer present, (b) close-up of the same RHI scan from the July 31st, 2012 rain event

4.2 Light Rain Event

This rain event occurred on August 24th, 2012 as described in Section 1.3.3.2. The melting layer was noticed around 19:31:18 UTC. Figure 4.6 (a) shows a reflectivity RHI scan of the rain event taken at 14.9° in azimuth. Figure 4.6 (b) shows a close-up of the same scan where the melting layer, identified with an ellipse, can be better appreciated. In this particular scan, the melting layer height is four thousand five hundred and ninety seven meters (4,597 m).

The average top height of the melting layer for this event was four thousand six hundred and fifty three meters (4,653 m). The melting layer height on average for this event was found at four thousand five hundred and fifty seven meters (4,557 m). The average melting layer bottom height was four thousand four hundred and forty four meters (4,444 m). The average melting layer width was calculated to be two hundred and nine meters (209 m).

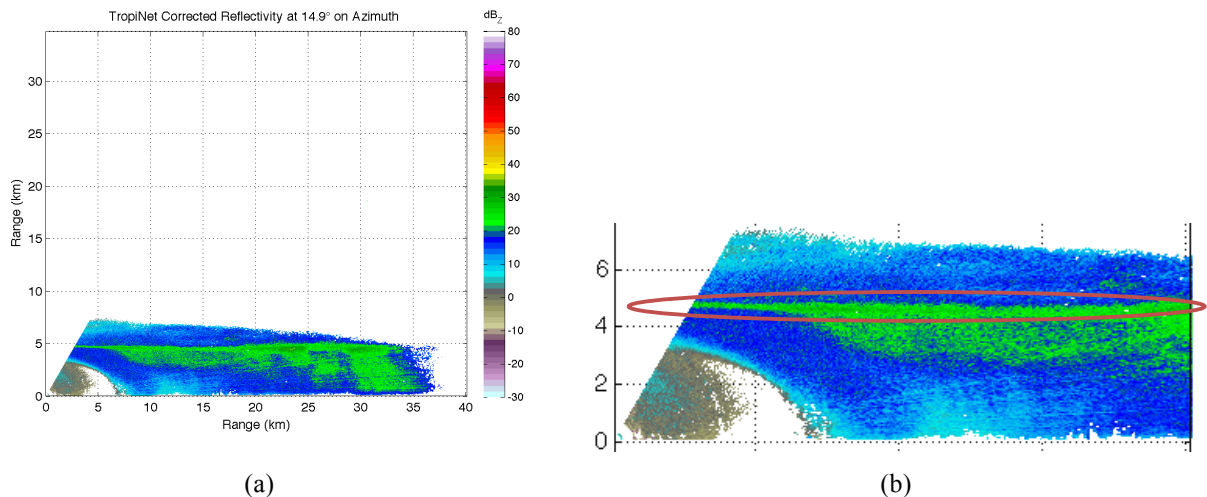


Figure 4.6 (a) Corrected reflectivity RHI scan with melting layer present, (b) close-up of the same RHI scan from the August 24th, 2012 rain event

The summary of the results is showed in Table 4.3 along with the 0°C isotherm height for this event.

Table 4.3 Average Characteristics of the Melting Layer for August 24th, 2012 Rain Event (m)

ML Top Height	ML Height	ML Bottom Height	ML Width	0°C Isotherm Height
4,653	4,557	4,444	209	4,765

The melting layer was corroborated using the cross-polar correlation, differential reflectivity, and specific differential phase of the data. Figure 4.7 (a) shows the cross-polar correlation of the same RHI scan presented in Figure 4.6. A close-up of the cross-polar correlation is showed in Figure 4.7 (b), where the drop in correlation of the data right in the melting layer, identified with an ellipse, is better appreciated. In Figure 4.8 (a) it can be seen the corrected differential reflectivity. To appreciate better the positive change in differential reflectivity, Figure 4.8 (b) shows a close-up. The change in differential reflectivity was found to be between one and four decibels (1-4 dB). Figure 4.9 (a) shows the specific differential phase. The values found in the melting layer for the specific differential phase were between one and three degrees pre kilometer (1-3 °/km). In the close-up of the specific differential phase, shown in Figure 4.9 (b), the melting layer is marked with an ellipse.

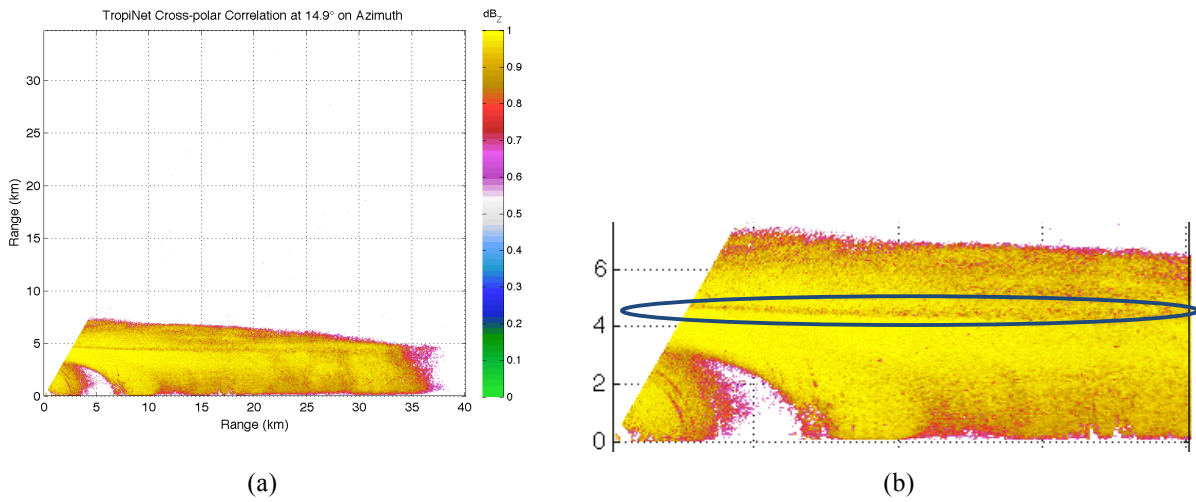


Figure 4.7 (a) Cross-polar correlation RHI scan with melting layer present, and (b) close-up of the same RHI scan from the August 24th, 2012 rain event

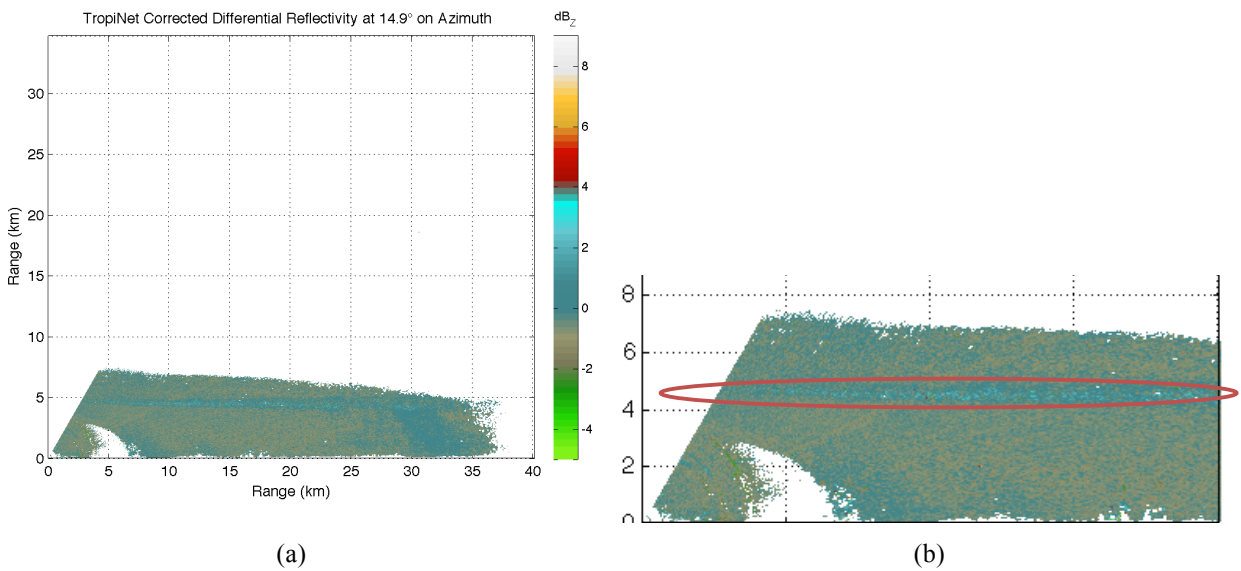


Figure 4.8 (a) Corrected differential reflectivity RHI scan with melting layer present, and (b) close-up of the same RHI scan from the August 24th, 2012 rain event

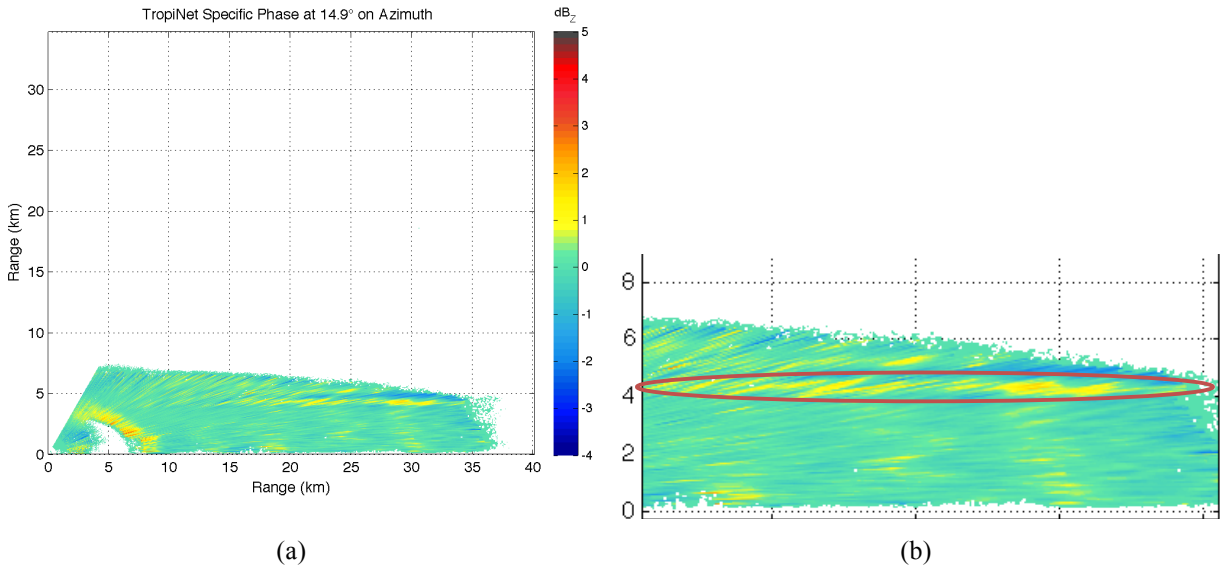


Figure 4.9 (a) Specific differential phase RHI scan with melting layer present, and (b) close-up of the same RHI scan from the August 24th, 2012 rain event

In this particular event it is also possible to identify the melting layer from a PPI scan. Figure 4.10 (a) shows a PPI scan of the reflectivity, (b) a PPI scan of the cross-polar correlation, (c) a PPI scan of the corrected differential reflectivity, and (d) a PPI scan of the specific differential phase where the melting layer, identified with an arrow, can be seen like a O-ring segment.

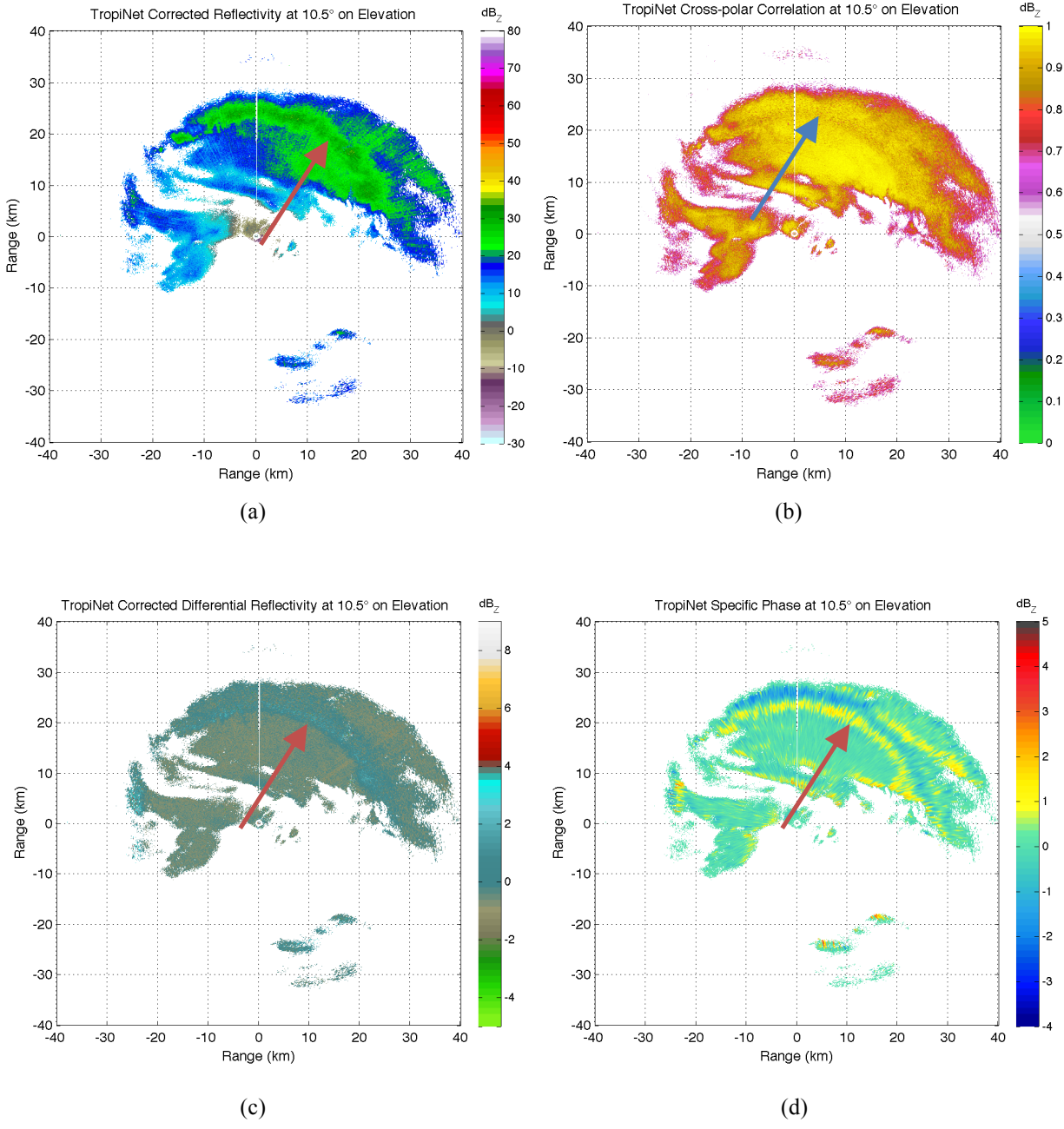


Figure 4.10 (a) PPI scan of the corrected reflectivity, (b) PPI scan of cross-polar correlation, (c) PPI scan of corrected differential reflectivity, and (d) PPI scan of specific differential phase from the August 24th, 2012 rain event

4.3 Mixed Moderate Rain Event

This rain event occurred on August 25th, 2012 as described in Section 1.3.3.3. The melting layer was noticed around 04:08:17 UTC. Figure 4.11 (a) shows a reflectivity RHI scan of the rain event taken at 75.0° in azimuth. Figure 4.11 (b) shows a close-up of the same scan where the melting layer, identified with an ellipse, can be better appreciated. It is intriguing how in this event in the first twenty kilometers the melting layer is appreciable and in the other twenty kilometers the convective rain destroys it. In this particular scan, the melting layer height is four thousand five hundred and seventy two meters (4,572 m).

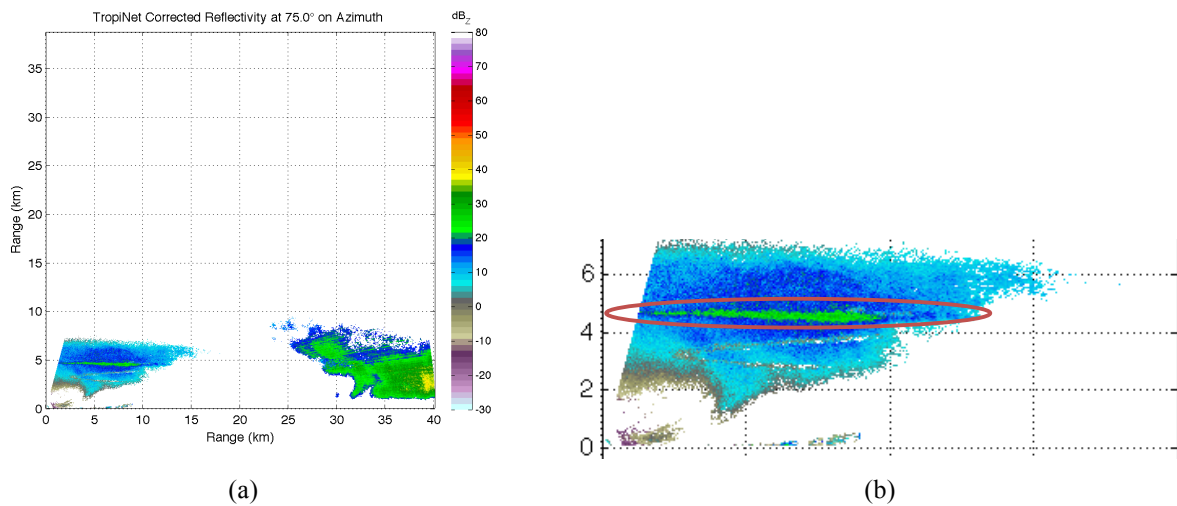


Figure 4.11 (a) Corrected reflectivity RHI scan with melting layer present, (b) close-up of the same RHI scan from the August 25th, 2012 rain event

The average top height of the melting layer for this event was four thousand six hundred and seventeen meters (4,617 m). The melting layer height on average for this event was found at four thousand five hundred and sixteen meters (4,516 m). The average melting layer bottom

height was four thousand four hundred and thirteen meters (4,413 m). The average melting layer width was calculated to be two hundred and four meters (204 m). The summary of the results is showed in Table 4.4 along with the 0°C isotherm height for this event.

Table 4.4 Average Characteristics of the Melting Layer for August 25th, 2012 Rain Event (m)

ML Top Height	ML Height	ML Bottom Height	ML Width	0°C Isotherm Height
4,617	4,516	4,413	204	4,737

The melting layer was corroborated using the cross-polar correlation, differential reflectivity, and specific differential phase of the data. Figure 4.12 (a) shows the cross-polar correlation of the same RHI scan presented in Figure 4.11. A close-up of the cross-polar correlation is showed in Figure 4.12 (b), where the drop in correlation of the data right in the melting layer, identified with an ellipse, is better appreciated. In Figure 4.13 (a) it can be seen the corrected differential reflectivity. To appreciate better the positive change in differential reflectivity, Figure 4.13 (b) shows a close-up. The change in differential reflectivity was found to be between one and four decibels (1-4 dB). Figure 4.14 (a) shows the specific differential phase. The values found in the melting layer for the specific differential phase were between one and three degrees pre kilometer (1-3 °/km). In the close-up of the specific differential phase, shown in Figure 4.14 (b), the melting layer is marked with an ellipse.

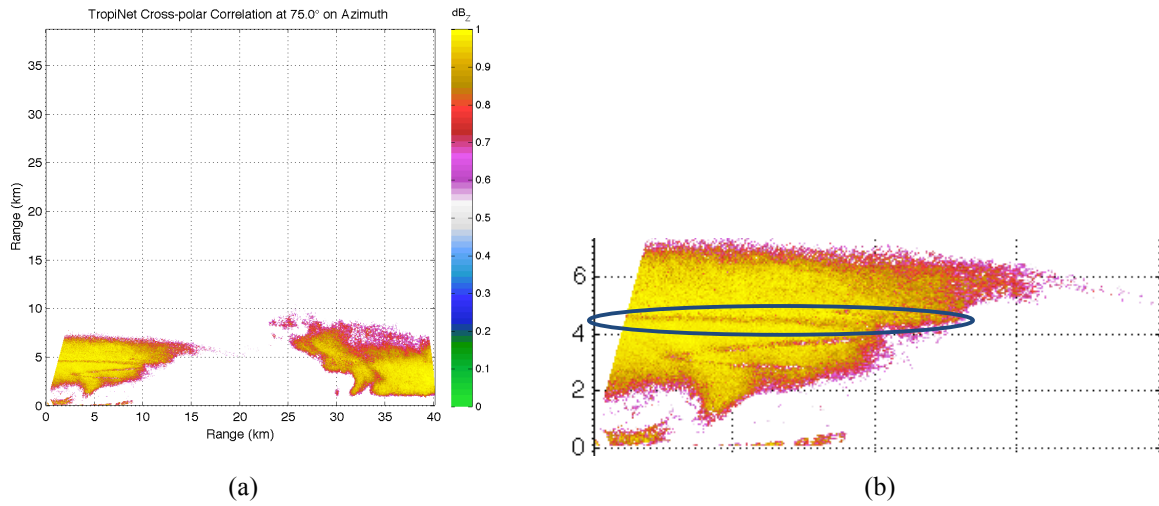


Figure 4.12 (a) Cross-polar correlation RHI scan with melting layer present, and (b) close-up of the same RHI scan from the August 25th, 2012 rain event

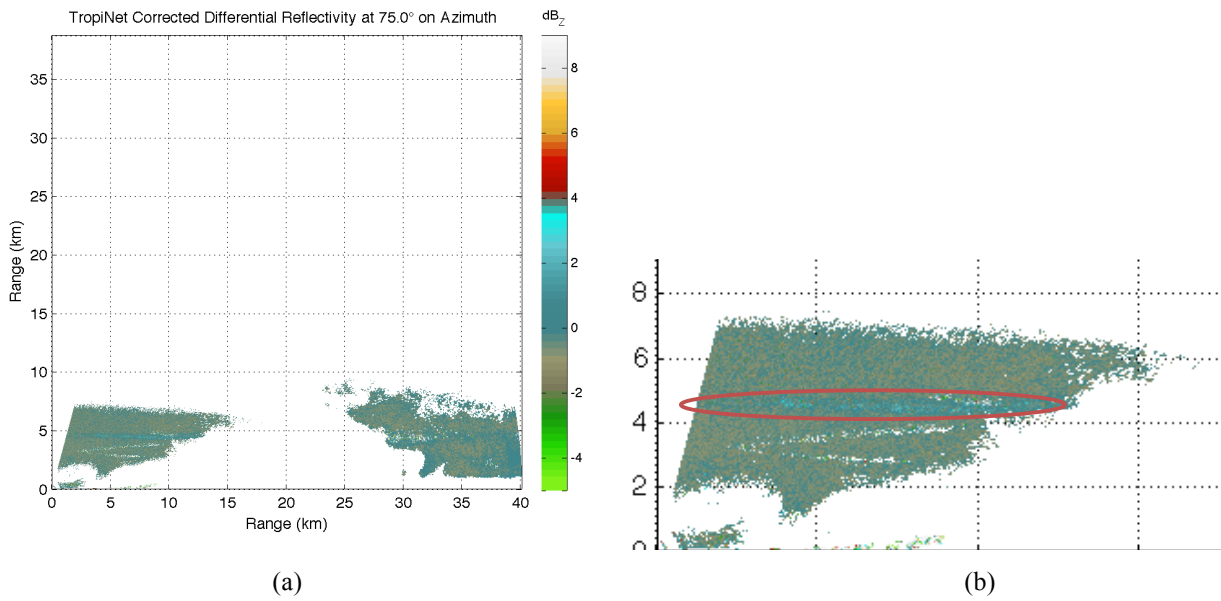


Figure 4.13 (a) Corrected differential reflectivity RHI scan with melting layer present, and (b) close-up of the same RHI scan from the August 25th, 2012 rain event

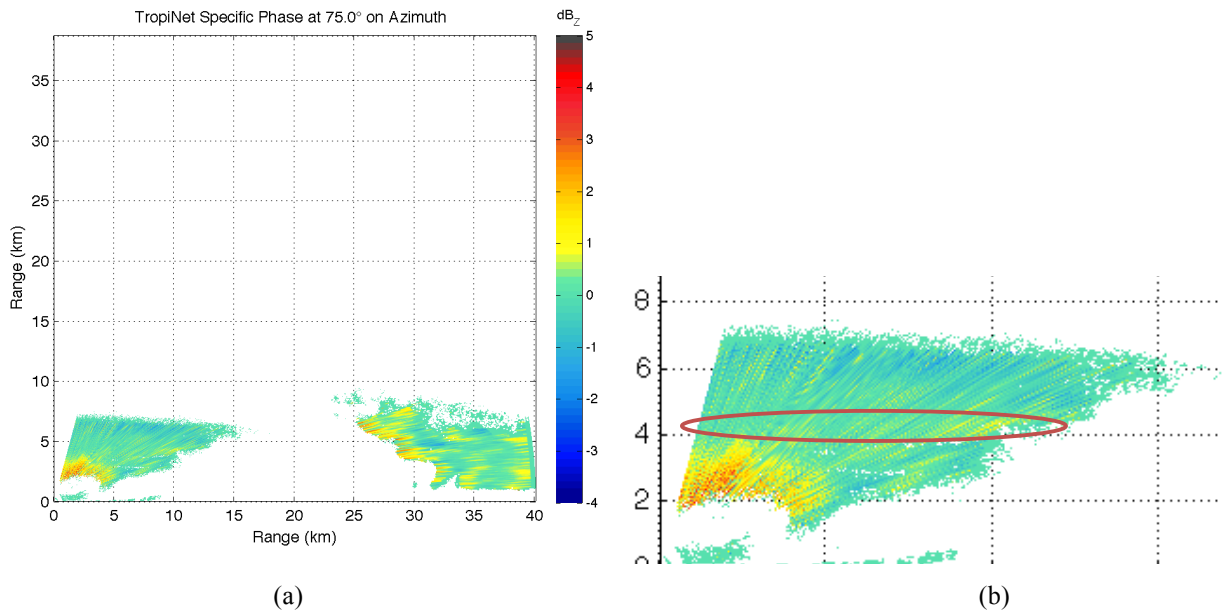


Figure 4.14 (a) Specific differential phase RHI scan with melting layer present, and (b) close-up of the same RHI scan from the August 25th, 2012 rain event

In this particular event it is also possible to identify the melting layer from a PPI scan. Figure 4.15 (a) shows a PPI scan of the reflectivity, (b) a PPI scan of the cross-polar correlation, (c) a PPI scan of the corrected differential reflectivity, and (d) a PPI scan of the specific differential phase where the melting layer, identified with an arrow, can be seen like an O-ring.

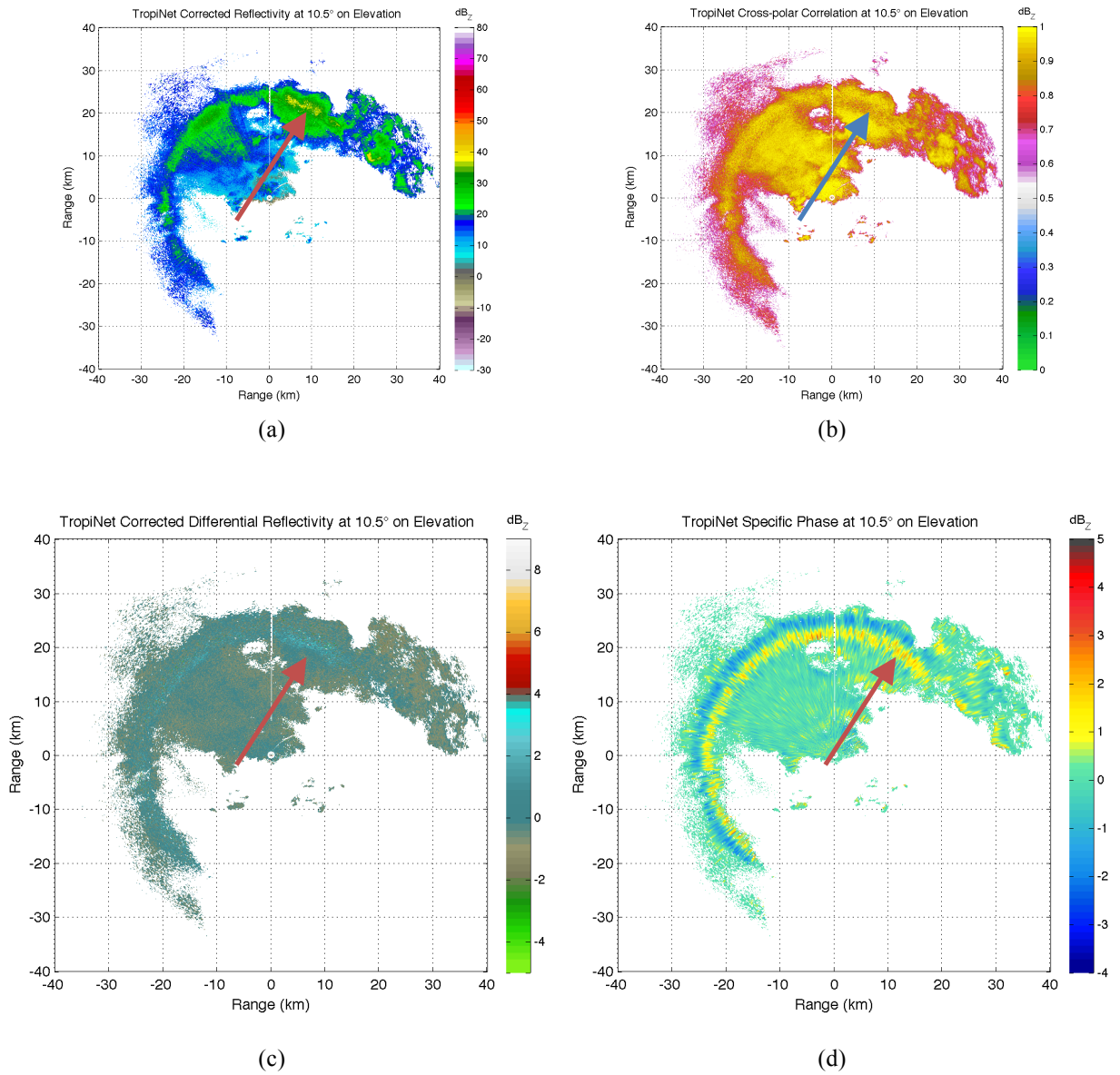


Figure 4.15 (a) PPI scan of the corrected reflectivity, (b) PPI scan of cross-polar correlation, (c) PPI scan of corrected differential reflectivity, and (d) PPI scan of specific differential phase from the August 25th, 2012 rain event

CHAPTER V

5 Conclusions

5.1 Summary

This study has confirmed that the melting layer forms in the Caribbean Tropic, specifically in the western coast of Puerto Rico. Achieving its main goal, using the vertical bidirectional sector scan technique. Without the polarimetric radar would not have been possible to complete this research because we do not have a radiometer to confirm the presence of the melting layer. Since the radar is polarimetric, it was possible to use the polarimetric products the radar gives. The main polarimetric product used to corroborate the presence of the melting layer was the cross-polar correlation due to its clear change in the melting layer on every scan.

The melting layer was only found in three of the fifty rain events studied. This means, that for the period of this study, the melting layer only appears on six percent (6%) of the rain events occurring in the western coast of Puerto Rico. Compared with the statistics presented in (*Jaiswal et al.*, 2010), the occurrence of the melting layer in the western coast of Puerto Rico is low. The features of the three rain events were different light, strong convective, and mixed which did not showed any particular pattern to conclude that the melting layer will be present depending on the type of precipitation.

Even though 6% may appear as a significant quantity to consider the effects in rain precipitation forecast, the height of the melting layer is too high to be in the radar's beam path, even for the long-range NEXRAD radar located approximately one hundred kilometers (100 km) east from the TropiNet-1. The range of the TropiNet radars is forty kilometers (40 km) and the normal operational elevation angles, especially for QPE, are 1.5°, 3.0°, and 4.5°. Even at 4.5° of elevation the radar beam does not reach the bottom height of the melting layer. To make the TropiNet-1 radar reach the bottom height of the melting layer at forty kilometers of range, it has to be operated between 6° and 7° on elevation. It is possible that long-range radars such as the NWS NEXRAD could be affected by the melting layer, as presented in this study, for ranges above one hundred and fifty five kilometers (155 km) approximately. So, combining the characteristics of the melting layer with its occurrence, it is determined that is not necessary to apply attenuation correction algorithms or QPE error correction algorithms due to the melting layer.

5.2 Future Work

To continue with this research, it is necessary to make the processing algorithms more automated. In this way, the human error variable is more controlled. The logic order of the algorithms can be change to make them more efficient. With these modifications, the algorithms should be integrated in the radar used on the study to process the data in real time.

The most important goal for future work, is to make a long-term study of the melting layer in the western coast of Puerto Rico. This study should be at least two years to have a better understanding of the long-term fluctuations of the melting layer in the Caribbean Tropic.

References

Atkins, N. T. (2002). Conventional Radar Lecture Notes. Retrieved from http://apollo.lsc.vsc.edu/classes/remote/lecture_notes/radar/conventional/bright_band.html

Battan, L. J. (1962). *Radar Observes the Weather* (1st Ed.). Garden City, NY: Anchor Books.

Battan, L. J. (1973). *Radar Observation of the Atmosphere* (1st Ed.). Chicago, IL: Univ. of Chicago Press.

Bellon, A., Zawadzki, I., & Fabry, F. (1997). Measurements of melting layer attenuation at X-band frequencies. *Radio Science*, 32(3), 943–955. doi:10.1029/97RS00492

Bringi, V. N., & Chandrasekar, V. (2001). *Polarimetric Doppler Weather Radar: Principles and Applications* (1st Ed.). Cambridge: Cambridge University Press.

Buderi, R. (1996). *The Invention that Changed the World* (1st Ed.). New York: Touchstone.

Cunningham, R. M. (1947). A DIFFERENT EXPLANATION OF THE “BRIGHT LINE”. *Journal of Meteorology*, 4(5), 163–163. doi:10.1175/1520-0469(1947)004<0163:ADEOTB>2.0.CO;2

Galvez, M. B., Colom, J., Chandrasekar, V., Junyent, F., Cruz-Pol, S., & Rodriguez, R. (2009). Salient features of the radar nodes in the Puerto Rico tropical weather testbed. *2009 IEEE International Geoscience and Remote Sensing Symposium* (pp. III–841–III–844). IEEE. doi:10.1109/IGARSS.2009.5417900

Hongping, L., & Chandrasekar, V. (2000). Classification of Hydrometeors Based on Polarimetric Radar Measurements: Development of Fuzzy Logic and Neuro-Fuzzy Systems, and In Situ Verification. *Journal of Atmospheric and Oceanic Technology*, 17(No. 2), 140–164. Retrieved from http://www.radar.colostate.edu/publications/chandra/ametsoc_35.htm

Jaiswal, S. J., Frederick, S. R., Neela, V. S., Rasheed, M., & Zaveri, L. (2010). Study of Radar Bright Band Over a Tropical Station. *9th Conference on Coastal Atmospheric and Oceanic Prediction and Processes*. Annapolis, MD.

Lhermitte, R. M., & Atlas, D. (1963). Doppler Fall Speed and Particle Growth in Stratiform Precipitation. *Tenth Weather Radar Conference* (pp. 297–302). Boston, MA, USA: American Meteorological Society.

Marshall, J. S., Langille, R. C., & Palmer, W. M. K. (1947). MEASUREMENT OF RAINFALL BY RADAR. *Journal of Meteorology*, 4(6), 186–192. doi:10.1175/1520-0469(1947)004<0186:MORBR>2.0.CO;2

Matrosov, S. Y., Clark, K. A., & Kingsmill, D. E. (2007). A Polarimetric Radar Approach to Identify Rain, Melting-Layer, and Snow Regions for Applying Corrections to Vertical Profiles of Reflectivity. *Journal Of Applied Meteorology And Climatology*, 46(2), 154–166. doi:10.1175/JAM2508.1

Okamoto, K., Sasaki, H., Deguchi, E., & Thurai, M. (2004). Bright Band Height Statistics Observed by the TRMM Precipitation Radar. *2nd TRMM International Science Conference*. Tokio, Japan.

Oolman, L. (University of W. D. of A. S. (2012). Atmospheric Soundings. Retrieved from <http://www.weather.uwyo.edu/upperair/sounding.html>

Rinehart, R. E. (2010). *Radar for Meteorologists* (5th Ed.). Nevada, Mo: Rinehart Publications.

Seliga, T. A., & Bringi, V. N. (1976). Potential use of radar differential reflectivity measurements at orthogonal polarizations for measuring precipitation. *Journal of Applied Meteorology*, 15(no. 1), 69–76. Retrieved from http://digitool.library.colostate.edu/R/?func=dbin-jump-full&object_id=171176&local_base=GEN01

Skolnik, M. I. (2001). *Introduction to Radar Systems* (3rd Ed.). New York: McGraw-Hill.

Smyth, T. J., & Illingworth, A. J. (1998). Radar estimates of rainfall rates at the ground in bright band and non-bright band events. *Quarterly Journal of the Royal Meteorological Society*, 124(551), 2417–2434. doi:10.1002/qj.49712455112

Tan, J., & Goddard, J. W. F. (1995). The Use of Dual-Polarization Techniques for Bright Band Detection with PPI-Based Radars. *IEE Colloquium on Radar Meteorology* (Vol. 1995, pp. 11–11). IEE. doi:10.1049/ic:19950204

White, A. B., Gattas, D. J., Strem, E. T., Ralph, F. M., & Neiman, P. J. (2002). An Automated Brightband Height Detection Algorithm for Use with Doppler Radar Spectral Moments. *Journal of Atmospheric and Oceanic Technology*, 19(5), 687–697. doi:10.1175/1520-0426(2002)019<0687:AABHDA>2.0.CO;2

APPENDIX

Appendix A: Data Processing Program Source Code

```
%%%%%%%%%%%%%%%%%%%%%%%%%%%%%%%%%%%%%%%%%%%%%%%%%%%%%%%%%%%%%%%%%%%%%%%%%
%       PNG Generator from NetCDF file       %
%               By                           %
%       José J. Rosario Colón               %
%       Created on March 5, 2013            %
%       Last Modified on April 3, 2013     %
%%%%%%%%%%%%%%%%%%%%%%%%%%%%%%%%%%%%%%%%%%%%%%%%%%%%%%%%%%%%%%%%%%%%%%%%%

close all
clear all
clc

%% Create the Necessary Folders %%

Path = input('Please specify the path of the folder you want to convert: ',
's');
PNG_path = [Path, 'PNG/'];
CDR_path = [PNG_path, 'Corrected Differential Reflectivity/'];
CR_path = [PNG_path, 'Corrected Reflectivity/'];
RhoHV_path = [PNG_path, 'Cross-polar Correlation/'];
SP_path = [PNG_path, 'Specific Phase/'];

v = exist(PNG_path, 'dir'); %Verifies if the PNG folder exist%

if v ~= 7 % If the folder doesn't exist, it creates the folder%

    mkdir(Path, 'PNG')

end

v = exist(CDR_path, 'dir'); %Verifies if the Corrected Differential
Reflectivity folder exist%

if v ~= 7 % If the folder doesn't exist, it creates the folder%

    mkdir(PNG_path, 'Corrected Differential Reflectivity')

end

v = exist(CR_path, 'dir'); %Verifies if the Corrected Reflectivity folder
exist%

if v ~= 7 % If the folder doesn't exist, it creates the folder%

    mkdir(PNG_path, 'Corrected Reflectivity')
```

```

end

v = exist(RhoHV_path,'dir'); %Verifies if the Differential Phase folder
exist%

if v ~= 7 % If the folder doesn't exist, it creates the folder%

    mkdir(PNG_path,'Cross-polar Correlation')

end

v = exist(SP_path,'dir'); %Verifies if the Specific Phase folder exist%

if v ~= 7 % If the folder doesn't exist, it creates the folder%

    mkdir(PNG_path,'Specific Phase')

end

%% Generate the List of Files %%

File_list = dir(Path);
m = size(File_list,1);
dir(Path)
n = str2double(input('Please enter the ID number of the file with which you
want to begin: ', 's'));

%% For Loop %%

for j = n : m

    s = [sprintf('\n'),'Processing file number ',num2str(j - n + 1),' of
',num2str(m - n + 1),sprintf('\n')];
    disp(s)

%% Open the NetCDF File and Load its Variables %%

    File_name = [Path,File_list(j).name];
    ncid = netcdf.open(File_name,'NC_NOWRITE'); %Opens the NetCDF file%

    Az_id = netcdf.inqVarID(ncid,'Azimuth'); %Reads the ID number of the
variable Azimuth%
    Az_set = netcdf.getVar(ncid,Az_id); % Reads and creates the Azimuth
variable matrix%

    El_id = netcdf.inqVarID(ncid,'Elevation'); %Reads the ID number of the
variable Elevation%
    El_set = netcdf.getVar(ncid,El_id); % Reads and creates the Elevation
variable matrix%

    Ur_id = netcdf.inqVarID(ncid,'Reflectivity'); %Reads the ID number of the
variable Uncorrected Reflectivity%

```

```

Ur_set = double(netcdf.getVar(ncid,Ur_id)); % Reads and creates the
Uncorrected Reflectivity variable matrix%

CZdr_id = netcdf.inqVarID(ncid,'CorrectedDifferentialReflectivity');
%Reads the ID number of the variable Corrected Differential Reflectivity%
CZdr_set = double(netcdf.getVar(ncid,CZdr_id)); % Reads and creates the
Corrected Differential Reflectivity variable matrix%

PhiDP_id = netcdf.inqVarID(ncid,'UnfoldedDifferentialPhase'); %Reads the
ID number of the variable Differential Phase%
PhiDP_set = double(netcdf.getVar(ncid,PhiDP_id)); % Reads and creates the
Differential Phase variable matrix%

RhoHV_id = netcdf.inqVarID(ncid,'CrossPolCorrelation'); %Reads the ID
number of the variable Copolar Correlation%
RhoHV_set = double(netcdf.getVar(ncid,RhoHV_id)); % Reads and creates the
Copolar Correlation variable matrix%

KDP_id = netcdf.inqVarID(ncid,'SpecificPhase'); %Reads the ID number of
the variable Specific Phase%
KDP_set = double(netcdf.getVar(ncid,KDP_id)); % Reads and creates the
Specific Phase variable matrix%

GW_id = netcdf.inqVarID(ncid,'GateWidth'); %Reads the ID number of the
variable Gate Width%
GW_set = netcdf.getVar(ncid,GW_id); % Reads and creates the Gate Width
variable matrix%

%% Simple Attenuation Correction %%

[a b] = size(Ur_set);
Cr_set = zeros(a,b);

for i = 1 : length(Az_set)

    alpha = 0.25;

    Zh = Ur_set(:,i);
    Phidp = PhiDP_set(:,i);
    Phidpl = -1*Phidp;
    Cr_set(:,i) = Zh + alpha*(Phidpl-Phidpl(1));

end

%% Possible Range of Values %%

KDP_set(KDP_set < -2) = -2; %Prevents the KDP value from being less than
-2%
KDP_set(KDP_set > 7) = 7; %Prevents the KDP value from being greater than
7%

Cr_set(Cr_set == -99900) = NaN; %Avoids that the minus infinity value
gates have color%

```

```

    Cr_set(RhoHV_set < 0.6) = NaN; %Prevents (filter) the uncorrelated
Reflectivity values from being displayed%
    CZdr_set(RhoHV_set < 0.6) = NaN; %Prevents (filter) the uncorrelated
Differential Reflectivity values from being displayed%
    KDP_set(RhoHV_set < 0.6) = NaN; %Prevents (filter) the uncorrelated
Specific Phase values from being displayed%
    RhoHV_set(RhoHV_set < 0.5) = NaN; %Prevents (filter) the meaningless
Cross-polar Correlation values from being displayed%

%% Verify if the Scan is a PPI or a RHI Scan %%

    El_7 = round(El_set(7) * 10) / 10; %Rounds the value to the first decimal
place%
    El_17 = round(El_set(17) * 10) /10; %Rounds the value to the first
decimal place%

    if El_7 == El_17

%% The File is a PPI Scan, Convert the Azimuths from Polar to Cartesian
Coordinates %%

        RangeToFirstGate = 0;
        drX = GW_set(1)/1000000;
        RngX = (drX*RangeToFirstGate):drX:(40.161-drX);
        AziX = Az_set;
        AziXr = -(AziX-90)*pi/180;
        [RngXM,AziXrM] = meshgrid(RngX,AziXr);
        X = RngXM.*cos(AziXrM);
        Y = RngXM.*sin(AziXrM);

%% Corrected Reflectivity Plot %%

        hh_1 = figure(1); %Creates an image of the Corrected Reflectivity%
        pcolor(X,Y,Cr_set')
        axis equal tight
            shading 'interp'
                caxis([-30 80])
                colorbar('FontSize',12)
                load('ReflectivityCmap','mycmap')
        set(hh_1,'Colormap',mycmap)
        set(gca,'FontSize',12)
            title(sprintf('TropiNet Corrected Reflectivity at %0.1f%c on
Elevation',El_set(7),char(176)), 'FontSize',12)
            xlabel('Range (km)', 'FontSize',12)
            ylabel('Range (km)', 'FontSize',12)
            grid on
            h = colorbar;
            hTitle = get(h,'Title');
            set(hTitle,'String','dB_Z')

        Save_name_1 = [Path,'PNG/Corrected
Reflectivity/',File_list(j).name,'.png'];
        saveas(hh_1,Save_name_1) %Saves the image%

```

```

%% Corrected Differential Reflectivity Plot %%

    hh_2 = figure(2); %Creates an image of the Corrected Differential
Reflectivity%
    pcolor(X,Y,CZdr_set')
    axis equal tight
    shading 'interp'
    caxis([-7 7])
    colorbar('FontSize',12)
    load('DiffRefCmap','mycmap')
    set(hh_2,'Colormap',mycmap)
    set(gca,'FontSize',12)
    title(sprintf('TropiNet Corrected Differential Reflectivity at
%0.1f%c on Elevation',El_set(7),char(176)),'FontSize',12)
    xlabel('Range (km)','FontSize',12)
    ylabel('Range (km)','FontSize',12)
    grid on
    h = colorbar;
    hTitle = get(h,'Title');
    set(hTitle,'String','dB_Z')

    Save_name_2 = [Path,'PNG/Corrected Differential
Reflectivity/',File_list(j).name,'.png'];
    saveas(hh_2,Save_name_2) %Saves the image%

%% Cross-polar Correlation Plot %%

    hh_3 = figure(3); %Creates an image of the Cross-polar Correlation%
    pcolor(X,Y,RhoHV_set')
    axis equal tight
    shading 'interp'
    caxis([0 1])
    colorbar('FontSize',12)
    load('DiffPhsCmap','mycmap')
    set(hh_3,'Colormap',mycmap)
    set(gca,'FontSize',12)
    title(sprintf('TropiNet Cross-polar Correlation at %0.1f%c on
Elevation',El_set(7),char(176)),'FontSize',12)
    xlabel('Range (km)','FontSize',12)
    ylabel('Range (km)','FontSize',12)
    grid on
    h = colorbar;
    hTitle = get(h,'Title');
    set(hTitle,'String','dB_Z')

    Save_name_3 = [Path,'PNG/Cross-polar
Correlation/',File_list(j).name,'.png'];
    saveas(hh_3,Save_name_3) %Saves the image%

%% Specific Phase Plot %%

    hh_4 = figure(4); %Creates an image of the Specific Phase%
    pcolor(X,Y,KDP_set')
    axis equal tight

```

```

        shading 'interp'
        caxis([-2 7])
        colorbar('FontSize',12)
        load('SpcPhsCmap','mycmap')
set(hh_4,'Colormap',mycmap)
set(gca,'FontSize',12)
        title(sprintf('TropiNet Specific Phase at %0.1f%c on
Elevation',El_set(7),char(176)), 'FontSize',12)
        xlabel('Range (km)', 'FontSize',12)
        ylabel('Range (km)', 'FontSize',12)
        grid on
        h = colorbar;
        hTitle = get(h, 'Title');
set(hTitle, 'String', 'dB_Z')

Save_name_4 = [Path, 'PNG/Specific Phase/', File_list(j).name, '.png'];
saveas(hh_4, Save_name_4) %Saves the image%

else

%% The File is a RHI Scan, Convert the Elevations from Polar to Cartesian
Coordinates %%

RangeToFirstGate = 0;
drX = GW_set(1)/1000000;
RngX = (drX*RangeToFirstGate):drX:(40.161-drX);
EleX = El_set;
EleXr = -(EleX-90)*pi/180;
[RngXM, EleXrM] = meshgrid(RngX, EleXr);
X = RngXM.*sin(EleXrM);
Y = RngXM.*cos(EleXrM);

%% Corrected Reflectivity Plot %%

hh_1 = figure(1); %Creates an image of the Corrected Reflectivity%
pcolor(X, Y, Cr_set')
axis equal tight
        shading 'interp'
        caxis([-30 80])
        colorbar('FontSize',12)
        load('ReflectivityCmap','mycmap')
set(hh_1, 'Colormap', mycmap)
set(gca, 'FontSize', 12)
        title(sprintf('TropiNet Corrected Reflectivity at %0.1f%c on
Azimuth', Az_set(7), char(176)), 'FontSize', 12)
        xlabel('Range (km)', 'FontSize', 12)
        ylabel('Range (km)', 'FontSize', 12)
        grid on
        h = colorbar;
        hTitle = get(h, 'Title');
set(hTitle, 'String', 'dB_Z')

Save_name_1 = [Path, 'PNG/Corrected
Reflectivity/', File_list(j).name, '.png'];
saveas(hh_1, Save_name_1) %Saves the image%

```

```

%% Corrected Differential Reflectivity Plot %%

    hh_2 = figure(2); %Creates an image of the Corrected Differential
Reflectivity%
    pcolor(X,Y,CZdr_set')
    axis equal tight
    shading 'interp'
    caxis([-7 7])
    colorbar('FontSize',12)
    load('DiffRefCmap','mycmap')
    set(hh_2,'Colormap',mycmap)
    set(gca,'FontSize',12)
    title(sprintf('TropiNet Corrected Differential Reflectivity at
%0.1f%c on Azimuth',Az_set(7),char(176)), 'FontSize',12)
    xlabel('Range (km)', 'FontSize',12)
    ylabel('Range (km)', 'FontSize',12)
    grid on
    h = colorbar;
    hTitle = get(h, 'Title');
    set(hTitle, 'String', 'dB_Z')

    Save_name_2 = [Path, 'PNG/Corrected Differential
Reflectivity/', File_list(j).name, '.png'];
    saveas(hh_2, Save_name_2) %Saves the image%

%% Cross-polar Correlation Plot %%

    hh_3 = figure(3); %Creates an image of the Cross-polar Correlation%
    pcolor(X,Y,RhoHV_set')
    axis equal tight
    shading 'interp'
    caxis([0 1])
    colorbar('FontSize',12)
    load('DiffPhsCmap','mycmap')
    set(hh_3,'Colormap',mycmap)
    set(gca,'FontSize',12)
    title(sprintf('TropiNet Cross-polar Correlation at %0.1f%c on
Azimuth',Az_set(7),char(176)), 'FontSize',12)
    xlabel('Range (km)', 'FontSize',12)
    ylabel('Range (km)', 'FontSize',12)
    grid on
    h = colorbar;
    hTitle = get(h, 'Title');
    set(hTitle, 'String', 'dB_Z')

    Save_name_3 = [Path, 'PNG/Cross-polar
Correlation/', File_list(j).name, '.png'];
    saveas(hh_3, Save_name_3) %Saves the image%

%% Specific Phase Plot %%

    hh_4 = figure(4); %Creates an image of the Specific Phase%
    pcolor(X,Y,KDP_set')
    axis equal tight

```

```

        shading 'interp'
        caxis([-2 7])
        colorbar('FontSize',12)
        load('SpcPhsCmap','mycmap')
set(hh_4,'Colormap',mycmap)
set(gca,'FontSize',12)
        title(sprintf('TropiNet Specific Phase at %0.1f%c on
Azimuth',Az_set(7),char(176)),'FontSize',12)
        xlabel('Range (km)','FontSize',12)
        ylabel('Range (km)','FontSize',12)
        grid on
        h = colorbar;
        hTitle = get(h,'Title');
set(hTitle,'String','dB_Z')

Save_name_4 = [Path,'PNG/Specific Phase/',File_list(j).name,'.png'];
saveas(hh_4,Save_name_4) %Saves the image%

end

netcdf.close(ncid) %Closes the NetCDF file%

end

```

Appendix B: Vertical Profile of Reflectivity Program Source Code

```
%%%%%%%%%%%%%%%%%%%%%%%%%%%%%%%%%%%%%%%%%%%%%%%%%%%%%%%%%%%%%%%%%%%%%%%%%
%       VPR Generator from NetCDF file       %
%               By                           %
%       José J. Rosario Colón               %
%       Created on March 5, 2013           %
%       Last Modified on April 3, 2013     %
%%%%%%%%%%%%%%%%%%%%%%%%%%%%%%%%%%%%%%%%%%%%%%%%%%%%%%%%%%%%%%%%%%%%%%%%%

close all
clear all
clc

%% Create the Necessary Folders %%

Path = input('Please specify the path of the folder you want to convert: ',
's');
VPR_path = [Path, 'VPR/'];

v = exist(VPR_path, 'dir'); %Verifies if the VPR folder exist%

if v ~= 7 %If VPR folder doesn't exist, it creates the folder%

    mkdir(Path, 'VPR')

end

%% Generate the List of Files %%

File_list = dir(Path);
m = size(File_list,1);
dir(Path)
n = str2double(input('Please enter the ID number of the file with which you
want to begin: ', 's'));

%% For Loop %%

for j = n : m

    s = [sprintf('\n'), 'Processing file number ', num2str(j - n + 1), ' of
', num2str(m - n + 1), sprintf('\n')];
    disp(s)

%% Open the NetCDF File and Load its Variables %%

File_name = [Path, File_list(j).name];
ncid = netcdf.open(File_name, 'NC_NOWRITE'); %Opens the NetCDF file%
```

```

    Az_id = netcdf.inqVarID(ncid,'Azimuth'); %Reads the ID number of the
variable Azimuth%
    Az_set = netcdf.getVar(ncid,Az_id); % Reads and creates the Azimuth
variable matrix%

    El_id = netcdf.inqVarID(ncid,'Elevation'); %Reads the ID number of the
variable Elevation%
    El_set = netcdf.getVar(ncid,El_id); % Reads and creates the Elevation
variable matrix%

    Ur_id = netcdf.inqVarID(ncid,'Reflectivity'); %Reads the ID number of the
variable Uncorrected Reflectivity%
    Ur_set = double(netcdf.getVar(ncid,Ur_id)); % Reads and creates the
Uncorrected Reflectivity variable matrix%

    PhiDP_id = netcdf.inqVarID(ncid,'UnfoldedDifferentialPhase'); %Reads the
ID number of the variable Differential Phase%
    PhiDP_set = double(netcdf.getVar(ncid,PhiDP_id)); % Reads and creates the
Differential Phase variable matrix%

    RhoHV_id = netcdf.inqVarID(ncid,'CrossPolCorrelation'); %Reads the ID
number of the variable Copolar Correlation%
    RhoHV_set = double(netcdf.getVar(ncid,RhoHV_id)); % Reads and creates the
Copolar Correlation variable matrix%

    GW_id = netcdf.inqVarID(ncid,'GateWidth'); %Reads the ID number of the
variable Gate Width%
    GW_set = netcdf.getVar(ncid,GW_id); % Reads and creates the Gate Width
variable matrix%

%% Simple Attenuation Correction %%

    [a b] = size(Ur_set);
    Cr_set = zeros(a,b);

    for i = 1 : length(Az_set)

        alpha = 0.25;

        Zh = Ur_set(:,i);
        Phidp = PhiDP_set(:,i);
        Phidpl = -1*Phidp;
        Cr_set(:,i) = Zh + alpha*(Phidpl-Phidpl(1));

    end

%% Verify if the Scan is a PPI or a RHI Scan %%

    El_7 = round(El_set(7) * 10) / 10; %Rounds the value to the first decimal
place%
    El_17 = round(El_set(17) * 10) /10; %Rounds the value to the first
decimal place%

    if El_7 ~= El_17

```

```
%% The File is a RHI Scan, Convert the Elevations from Polar to Cartesian
Coordinates %%
```

```
RangeToFirstGate = 0;
drX = GW_set(1)/1000000;
RngX = (drX*RangeToFirstGate):drX:(20.0805-drX);
EleX = El_set;
EleXr = -(EleX-90)*pi/180;
[RngXM, EleXrM] = meshgrid(RngX, EleXr);
X = RngXM.*sin(EleXrM);
Y = RngXM.*cos(EleXrM);
```

```
%% Create the Vertical Profile of Reflectivity %%
```

```
VPR = zeros(a/2,b);

for i = 1 : a/2

    VPR(i,:) = Cr_set(i,:);

end
```

```
%% Possible Range of Values %%
```

```
VPR(VPR <= -10) = -10; %Avoids that the minus infinity value gates
distort the plot%
```

```
%% Vertical Profile of Reflectivity Plot %%
```

```
d = j - n + 1;
hh_j = figure(d); %Creates an image of the Vertical Profile of
Reflectivity%
plot(VPR',Y)
ylim([0 20])
title(sprintf('TropiNet Vertical Profile of Reflectivity at
%0.1f%c on Azimuth',Az_set(7),char(176)), 'FontSize',12)
xlabel('Reflectivity (dBZ)', 'FontSize',12)
ylabel('Range (km)', 'FontSize',12)
grid on

Save_name_1 = [Path, 'VPR/', File_list(j).name, '.png'];
saveas(hh_j, Save_name_1) %Saves the image%
```

```
end
```

```
netcdf.close(ncid) %Closes the NetCDF file%
```

```
end
```